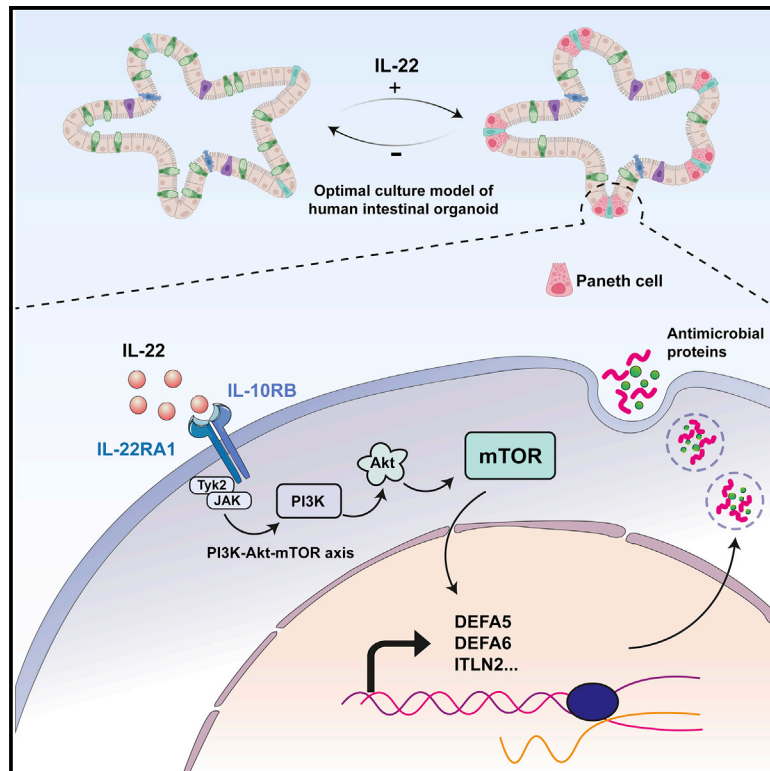


Optimized human intestinal organoid model reveals interleukin-22-dependency of paneth cell formation

Graphical abstract



Authors

Gui-Wei He, Lin Lin, Jeff DeMartino, ..., Thanasis Margaritis, Frank Holstege, Hans Clevers

Correspondence

h.clevers@hubrecht.eu

In brief

Generating a long-term organoid culture model that displays extensive budding and harbors all cell types of the human small intestine reveals mechanism of human Paneth cell differentiation by IL-22-mTOR signaling.

Highlights

- Optimized culture protocol for human intestinal organoids
- Organoids display extensive budding and harbor all cell types
- IL-22-mTOR signaling mediates human Paneth cell differentiation
- IL-22 induces expression of host defense genes in all cell types



Article

Optimized human intestinal organoid model reveals interleukin-22-dependency of paneth cell formation

Gui-Wei He,^{1,10} Lin Lin,^{1,2,10} Jeff DeMartino,² Xuan Zheng,³ Nadzeya Staliarova,^{4,5} Talya Dayton,¹ Harry Begthel,¹ Willine J. van de Wetering,⁶ Eduard Bodewes,² Jeroen van Zon,³ Sander Tans,³ Carmen Lopez-Iglesias,⁶ Peter J. Peters,⁶ Wei Wu,^{4,5,7} Daniel Kotlarz,⁸ Christoph Klein,⁸ Thanasis Margaritis,² Frank Holstege,² and Hans Clevers^{1,2,9,11,*}

¹Onco Institute, Hubrecht Institute, Royal Netherlands Academy of Arts and Sciences and University Medical Center, Uppsalalaan 8, Utrecht, 3584 CT, the Netherlands

²The Princess Maxima Center for Pediatric Oncology, 3584 CS Utrecht, the Netherlands

³AMOLF, Amsterdam, the Netherlands

⁴Biomolecular Mass Spectrometry and Proteomics, Bijvoet Center for Biomolecular Research and Utrecht Institute for Pharmaceutical Sciences, Utrecht University, Padualaan 8, 3584 CH Utrecht, the Netherlands

⁵Netherlands Proteomics Centre, Padualaan 8, 3584 CH Utrecht, the Netherlands

⁶The Maastricht Multimodal Molecular Imaging Institute, Maastricht University, 6229 ER Maastricht, the Netherlands

⁷Singapore Immunology Network (SiGN), ASTAR (Agency for Science, Technology and Research), Singapore

⁸Department of Pediatrics, Dr. von Hauner Children's Hospital, University Hospital, Ludwig Maximilian University Munich, Munich, Germany

⁹Present address: Pharma, Research and Early Development (pRED) of F. Hoffmann-La Roche Ltd, Basel, Switzerland

¹⁰These authors contributed equally

¹¹Lead contact

*Correspondence: h.clevers@hubrecht.eu

<https://doi.org/10.1016/j.stem.2022.08.002>

SUMMARY

Opposing roles have been proposed for IL-22 in intestinal pathophysiology. We have optimized human small intestinal organoid (hSIO) culturing, constitutively generating all differentiated cell types while maintaining an active stem cell compartment. IL-22 does not promote the expansion of stem cells but rather slows the growth of hSIOs. In hSIOs, IL-22 is required for formation of Paneth cells, the prime producers of intestinal antimicrobial peptides (AMPs). Introduction of inflammatory bowel disease (IBD)-associated loss-of-function mutations in the IL-22 co-receptor gene *IL10RB* resulted in abolishment of Paneth cells in hSIOs. Moreover, IL-22 induced expression of host defense genes (such as *REG1A*, *REG1B*, and *DMBT1*) in enterocytes, goblet cells, Paneth cells, Tuft cells, and even stem cells. Thus, IL-22 does not directly control the regenerative capacity of crypt stem cells but rather boosts Paneth cell numbers, as well as the expression of AMPs in all cell types.

INTRODUCTION

Interleukin-22, or IL-22, is produced by immune cells and mainly acts on epithelial cells. It thus represents a major communication channel between the immune system and specialized tissue cell types that express the IL-22 co-receptor complex. IL-22 has been implicated in multiple aspects of intestinal biology. It is believed to be an important driver of mucosal healing. A key study (largely based on murine *in vitro* organoid experiments) has proposed that IL-22 promotes tissue regeneration by directly increasing numbers and proliferative activity of intestinal stem cells (ISCs) (Lindemans et al., 2015). Yet, two recent mouse studies have suggested that IL-22 promotes regeneration by inducing proliferation of transit-amplifying cells (TAs) while suppressing ISC expansion and even inducing ISC apoptosis (Zha et al., 2019; Zwarycz et al., 2019). IL-22 has been positively evaluated as a potential therapy for epithelial injury in the mouse as occurring in inflammatory bowel disease (IBD) (Rothenberg

et al., 2019). In an alternative role, IL-22 has been reported to act by inducing barrier protection against pathogens through goblet cell differentiation and mucin secretion (Layunta et al., 2021; Sugimoto et al., 2008; Turner et al., 2013), production of anti-microbial proteins (AMPs) (Gaudino et al., 2021), and production of complement factors (Hasegawa et al., 2014).

The role of IL-22 in IBD has remained unresolved (Keir et al., 2020; Mizoguchi et al., 2018). In pre-clinical mouse models, blocking IL-22 production or neutralization of IL-22 by antibody improves intestinal inflammation (Eken et al., 2014; Reyes et al., 2016). Conversely, deficiency of IL-22 or IL-22 receptor leads to exacerbated colitis, while treatment with IL-22-Fc fusion protein improved inflammation in wild-type mice (Cox et al., 2012; Stefanich et al., 2018; Zenewicz et al., 2008). In IBD patients, persistent symptoms of barrier dysfunction and disease progression were observed in correlation with increased IL-22 levels in patients with IBD (Schmechel et al., 2008), suggesting a pathogenic role of IL-22 in IBD. Yet, another study has



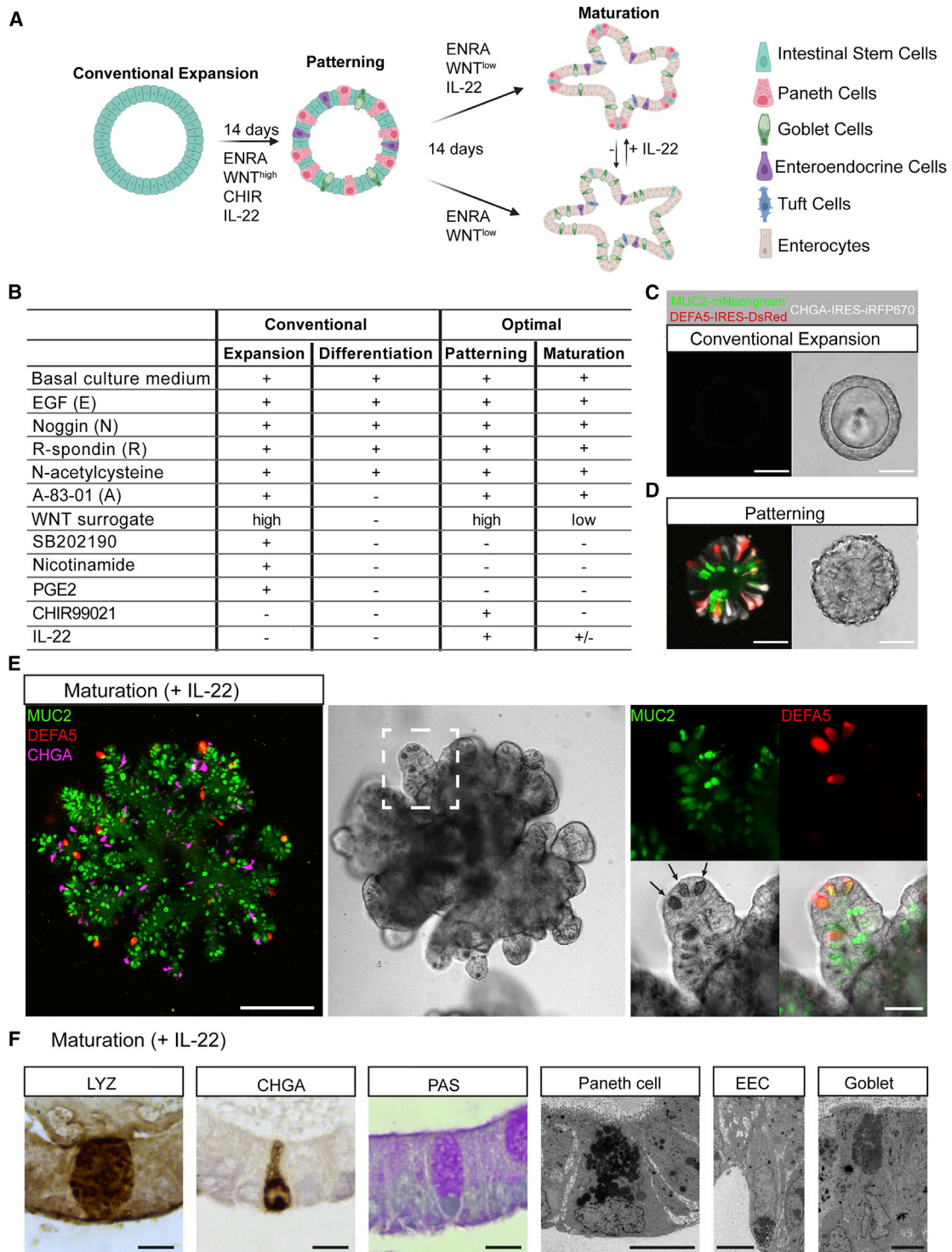


Figure 1. Optimal culture of human intestinal organoids with multi-differentiation capacity

(A) Schematics of optimal culture model for hSIOs. hSIOs are patterned from conventional expansion culture and maintained in maturation media.

(B) Medium composition comparison between conventional culture and optimal culture of hSIOs.

(C–E) Representative confocal images of hSIOs cultured in conventional expansion medium (C), patterning medium for 14 days (D), and maturation medium with IL-22 (E). Representative marker genes for Paneth (DEFA5, red), enteroendocrine (CHGA, white/magenta), and goblet (MUC2, green) cells are highlighted by

(legend continued on next page)

implied a protective role of IL-22 in IBD patients (Pelczar et al., 2016).

Small intestinal organoids (SIOs) provide an *in vitro* model to study the direct effects of biological regulators on primary epithelial cells in the absence of confounding factors (Sato et al., 2009, 2011b). While improved culture conditions have been described for human SIOs (Fujii et al., 2018; Jarde et al., 2020; Pleguezuelos-Manzano et al., 2020), cell type diversity and three-dimensional (3D) structure of human intestinal tissues are yet to be fully recapitulated. In particular, existing human organoid protocols essentially fail to produce extensive budding. The resulting organoids largely consist of progenitor cells, while mature Paneth cells remain rare or absent, even after removal of mitogenic growth factors. Of note, Paneth cells are crucial in modulating host defense by producing intestinal AMPs, such as lysozyme and defensins (Bevins and Salzman, 2011). The differentiation program of human Paneth cells is yet to be defined. Here, we establish an optimized human SIO protocol in which we probe the direct effects of IL-22 on the induction and gene expression of the various epithelial cell types of the human small intestinal epithelium, specifically focusing on ISCs and Paneth cells.

RESULTS

Optimized culture of human intestinal organoids

When we explored the effects of IL-22 on mouse SIO cultures, we failed to reproduce the reported increase in stem cell expansion and in organoid growth (Figures S1A–S1E; Lindemans et al., 2015). Similar observations were made using conventional culture of human SIOs (hSIOs) (Figures S1F–S1H). Prompted by this, we sought to optimize the hSIO culture protocol in order to document effects of IL-22 on all intestinal cell types. Starting from hSIOs grown in our conventional expansion medium (Sato et al., 2011a), we developed a two-step patterning-maturation protocol (Figure 1A). Conventional expansion medium sustains growth of “bud-less” organoids that largely consist of stem cells and enterocyte progenitors (Sato et al., 2011a), while removal of mitogenic factors from the medium drives these cells toward more mature enterocyte phenotypes (Sato et al., 2011a). Our step one patterning medium (Figure 1A) drove differentiation of hSIOs toward secretory lineages (Figure S2A). Following this 14-day patterning phase, step two was comprised of removal of CHIR99021 and reduction of Wnt3 (designated “maturation medium”) (Figure 1B). Maturation medium supported expansion of organoids with extensive crypt-like budding structures (Figure S2B).

We created a triple knock-in reporter organoid line to directly visualize different secretory cell types in live SIOs. Under these maturation conditions, goblet cells (MUC2-mNeon) (Artegiani et al., 2020) and enteroendocrine cells (EECs) (CHGA-IRES-iRFP) were scattered throughout the organoid structure (Figures 1C–1E and S2D). Paneth cells (DEFA5-IRES-DsRed) appeared when IL-22 was added and were mainly located at the

base of the buds recapitulating their localization in intestinal crypts *in vivo* (Figures 1C–1E and S2D). Addition of nicotinamide, SB202190, or prostaglandin E2 (PGE2) from the conventional culture medium in maturation cultures significantly blocked Paneth cell formation (Figure S2C). Staining with immunohistochemistry markers (goblet cell: periodic acid–Schiff [PAS], EEC: chromogranin A1 [CHGA], Paneth cell: lysozyme [LYZ]) and morphological characterization by transmission electron microscopy (TEM) confirmed the maturity of these secretory cell types (Figure 1F). When taken through our protocol, hSIOs were phenotypically stable during long-term culture in maturation medium and contained a diversity of small intestinal cell types (Figure S2E). Of note, matured SIOs can be derived from conventionally expanded SIOs, where the latter condition is compatible with the clonal expansion protocol used for genetic engineering (Fujii et al., 2015).

To provide a comprehensive view of the created cell diversity, matured organoids (grown in the presence of IL-22 for 14 days) were subjected to single-cell RNA sequencing (scRNA-seq) analyses. Our data captured 1,283 cells that clustered into 10 populations annotated by well-known markers. These included ISCs, two subclusters of TAs, early and late enterocytes, secretory progenitors, goblet cells, Paneth cells, EECs, and Tuft cells (Figures 2A, 2B, S3A and Table S2). Of note, it was not possible to distinguish Paneth cells from goblet cells via graph-based clustering alone. We therefore calculated a module score using the Paneth cell-specific markers DEFA5, DEFA6, PLA2G2A, PRSS2, REG3A, and ITLN2 to subcluster Paneth cells from goblet cells (Figure S3B). Also, the homozygous knock-in construct *DEFA5-IRES2-DsRed* contains a high GC-rich region (IRES2), which prohibits complete cDNA synthesis of *DEFA5* transcripts using oligo (dT) primer. This prohibited the detection of *DEFA5* expression at the mRNA level using oligo (dT) primer in 10X scRNA-seq (Figure S3B). Cells in the Paneth cell cluster expressed high levels of LYZ, another commonly used marker to identify Paneth cells (Figure S3B). Our organoid model recapitulated the clustering pattern of primary Paneth cells and goblet cells (Burclaff et al., 2022). In line with the previously observed requirement of non-epithelial Wnt signals in hSIOs culture (Sato et al., 2011a), no significant expression of any WNT family member was detected in human Paneth cells from our scRNA-seq data (Figure S4A). This result also agreed with human tissue scRNA-seq analyses (Burclaff et al., 2022; Buslinger et al., 2021). Indeed, exogenous Wnt was indispensable for maintaining hSIOs with mature Paneth cells (Figure S2B). This represented a fundamental difference between human and mouse intestine epithelium, as in the latter case Paneth cells support stem cells by secreting Wnt3 and Wnt11 (Sato et al., 2011b).

To outline the path of cell differentiation, we performed RNA velocity analysis (Bergen et al., 2020) and lineage trajectory reconstruction (Figures S4B–S4D). This revealed a differentiation path from ISC-derived TA2 cells to early enterocytes, which further differentiated into late enterocytes (Figure S4D). Meanwhile, Paneth cells and goblet cells shared a common path,

fluorescent reporters. Right: zoom-in image of the budding crypt. The black arrowheads highlight the Paneth cells located at the crypt bottom. Scale bars (C and D), 50 μ m; (E) right scale bar, 50 μ m; left scale bar, 200 μ m. (F) Paneth (LYZ), enteroendocrine (CHGA), and goblet cells (PAS) in maturation medium (+IL-22)-cultured organoids detected by immunohistochemistry staining and transmission electron microscopy. Scale bars, 5 μ m. See also Figure S2.

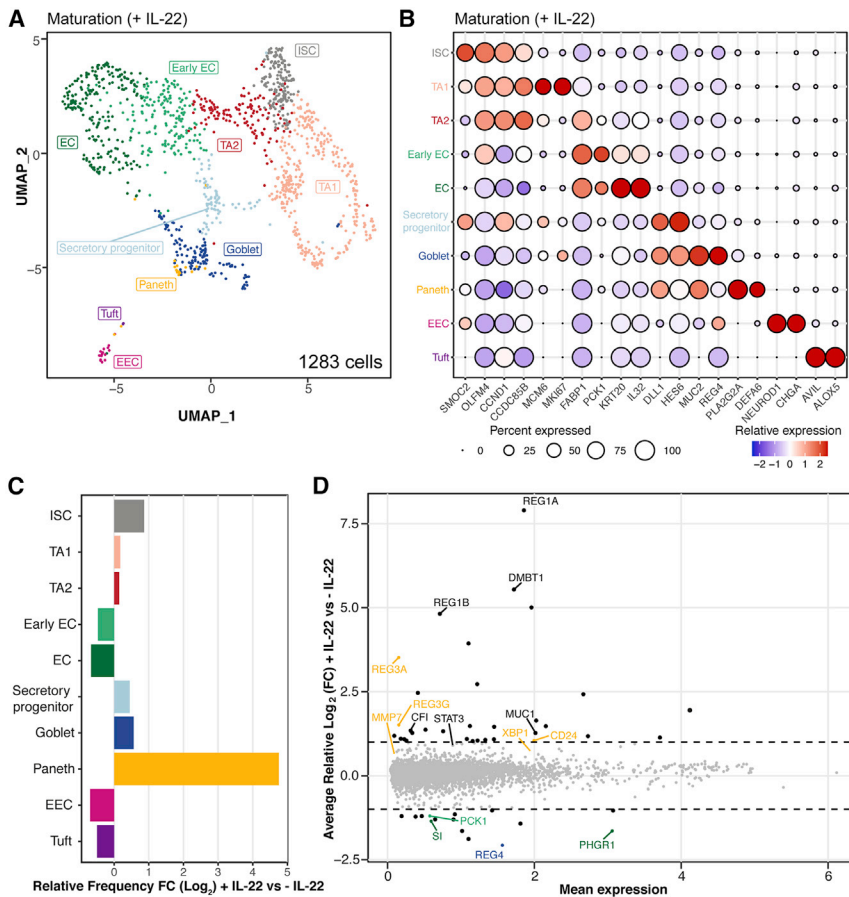


Figure 2. IL-22 regulates cellular diversity of hSIOs

(A) UMAP of maturation medium (+IL-22)-cultured organoids for 14 days from scRNA-seq analysis ($n = 1,283$ cells). Descriptive cluster labels are shown. ISC, intestinal stem cell; TA1, transit-amplifying cell stage 1; TA2, transit-amplifying cell stage 2; EC, enterocyte; EEC, enteroendocrine cell.

(B) Dot plot showing the relative expression and the percentage of cells expressing selected markers across scRNA-seq clusters. Two representative markers for each cluster are plotted.

(C) Bar plot showing the relative Log_2 fold change of cell populations in maturation medium-cultured organoids with or without the addition of IL-22.

(D) MA plot showing differentially expressed genes between maturation medium-cultured organoids with or without the addition of IL-22 by pseudobulk analysis of scRNA-seq. Representative marker genes for the different cell types are color-coded as in (C). See also Figures S3 and S4 and Tables S2 and S3.

originating from a shared population of ATOH1⁺ secretory progenitors (Figure S4D). This was consistent with the clustering pattern of Paneth cells and goblet cells (Figure 2A). Taken together, hSIOs cultured with our optimized protocol recapitulated the cell heterogeneity and differentiation dynamics of human intestinal crypts.

IL-22 does not promote intestinal regeneration

To evaluate the impact of IL-22 on cell diversity, we performed a scRNA-seq comparison between hSIOs cultured in maturation medium with and without addition of IL-22 (Figures 2A and S3C). IL-22 increased the relative ratio of ISCs (Figure 2C) but decreased the total number of live cells, leaving the absolute number of ISCs unchanged (Figure 3A) while significantly reducing the efficiency of organoid formation (Figure 3B). Moreover, IL-22 decreased organoid budding and increased cell death, indicating a deleterious role of IL-22 in long-term culture of hSIOs (Figures 3C, 3D, and 3F). IL-22 did not promote cell proliferation (Figure 3E). These observations were consistent with our results from mouse SIOs (Figures S1A–S1E) and hSIOs cultured in conventional expansion medium (Figures S1F–S1H). Collectively, our data indicated that IL-22 enhances neither the expansion of ISCs nor the growth of hSIOs, again challenging the notion of IL-22 promoting intestinal regeneration.

Furthermore, our scRNA-seq result showed that IL-22 strongly decreased the relative proportion of (early) enterocytes

(Figures 2C, 2D, and 3G), the most abundant differentiated cell type. In confirmation of this observation, IL-22 suppressed the expression of enterocyte-related genes such as ANPEP and CYP3A4 (Figure 3H).

IL-22 induces human Paneth cell differentiation

Paneth cells were almost absent in maturation medium upon removal of IL-22, indicating a role for IL-22 in human Paneth cell differentiation in these cultures (Figures 2C, 4A, 4B, S6E, and S6G). Addition of IL-22 to maturation medium induced the appearance of Paneth cells within a week, while withdrawal of IL-22 resulted in disappearance of Paneth cells within two weeks, in agreement with the lifetime of Paneth cells (Figure 4C). The percentages of goblet cells and EECs in organoids were not affected by IL-22, indicating that IL-22 specifically induces Paneth cell differentiation rather than driving overall secretory cell lineage commitment (Figure 4C). Patterned hSIOs could be passaged once a week and expanded in maturation media without IL-22 for >12 months, after which Paneth cells could still be induced efficiently by IL-22 (Figure S2E). This reversible phenotype identified IL-22 signaling as a key mediator of Paneth cell homeostasis.

This induction of Paneth cells was dose dependent and saturated at a low dosage of around 2 ng/ml (Figure 4D). IL-22 was the only Paneth cell inducer amongst a large panel of cytokines examined (Figures 4E and S5A). Similar to the ileal organoids used above (derived from three independent donors), IL-22 induced Paneth cells formation in organoids derived from duodenum (Figure S6H).

For direct comparison with previously established culture system reported with the presence of Paneth cells (Fujii et al., 2018), we cultured the Paneth cell reporter organoid line (DEFA5-IRES-DsRed) with this medium formula (designated as “Sato IF”), which uses a combination of IGF and FGF2 to replace epidermal

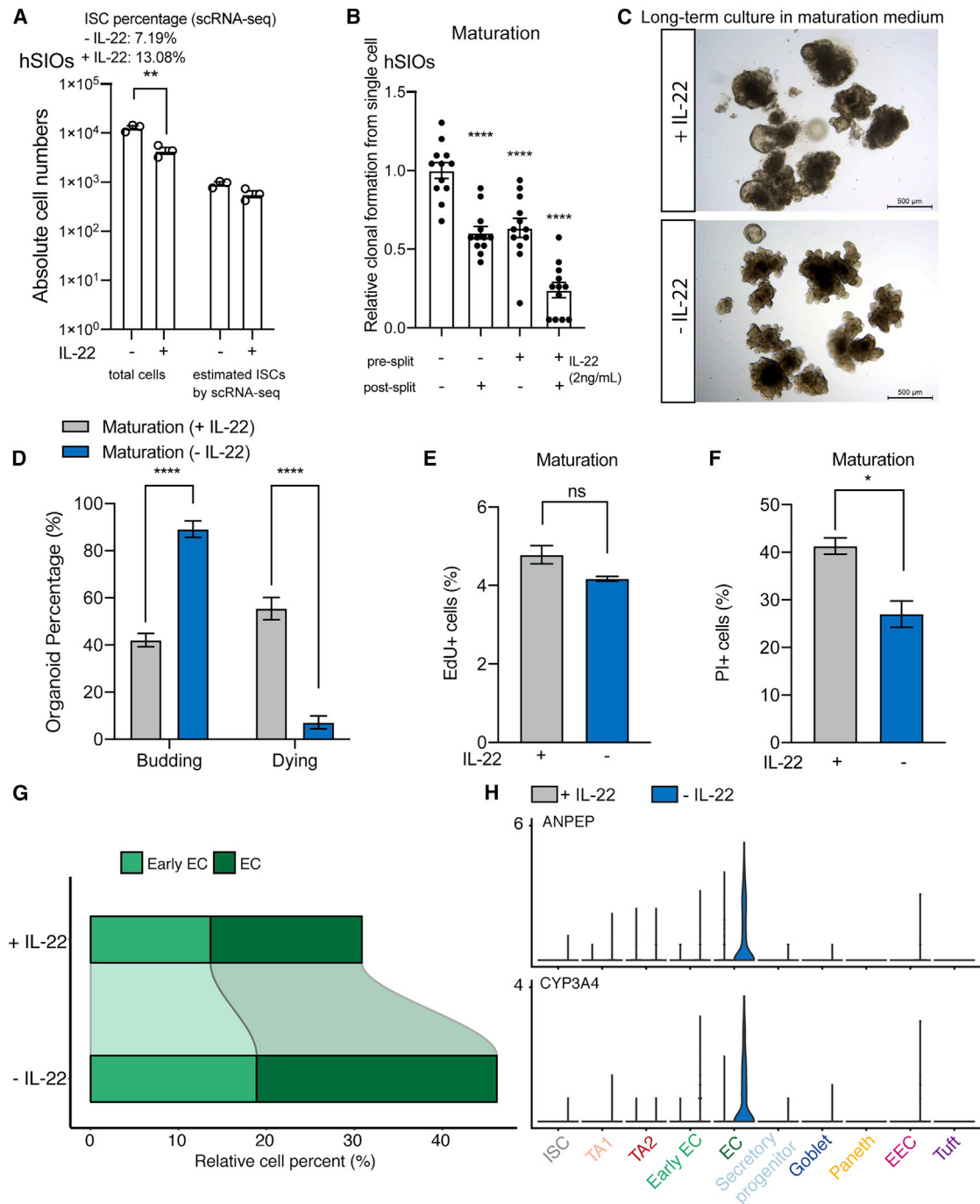


Figure 3. IL-22 inhibits growth of human intestinal organoids

(A) Bar plot showing the absolute total cell numbers and estimated ISC numbers of maturation medium-cultured organoids with or without the addition of IL-22 for 14 days.

Data are shown as mean \pm SEM. ****** $p < 0.01$; two-tailed unpaired t test, $n = 3$.

(B) Bar plot showing the relative clonal formation efficiency from single cells of maturation medium-cultured organoids in response to addition, or upon withdrawal, of IL-22 for 14 days.

Data are shown as mean \pm SEM. ******** $p < 0.0001$; one-way ANOVA compared with maturation medium-cultured organoids (-IL-22), $n = 12$ for each condition.

(C) Representative images of long-term maturation medium-cultured organoids (4 passages) with or without the addition of IL-22 for 28 days. Scale bars, 500 μ m.

(D) Quantification of the percentage of budding and dying organoids.
Data are shown as mean \pm SEM. ******** $p < 0.0001$; multiple t tests using two-stage linear step-up procedure of Benjamini, Krieger, and Yekutieli compared with maturation medium-cultured organoids (+IL-22) with $Q = 5\%$, images $n = 10$ for each condition.

(E) Cell proliferation as determined by FACS analysis of EdU positive cells.

(legend continued on next page)

growth factor (EGF). Fluorescence-activated cell sorting (FACS) analysis showed that DEFA5-positive Paneth cells remained very rare in IF-cultured organoids (Figure S5B). Importantly, IL-22 could still induce the appearance of Paneth cells in Sato IF medium at a low level (Figures S5A and S5B). Yet, organoids cultured with Sato IF + IL-22 did not form budding structures (Figure S5B).

To probe the origin of Paneth cells, we performed image-based real-time lineage tracking of the triple reporter line. Newly induced Paneth cells all derived from MUC2⁺ progenitor cells (Figures 4F and 4G), supporting the notion that Paneth cells and goblet cells share a common secretory progenitor population (Yang et al., 2001), which was also in accordance with our scRNA-seq analyses (Figure S4D). In contrast, IL-22 was not necessary for the presence of mouse Paneth cells *in vivo* and in mSIO culture *in vitro* (Gaudino et al., 2021; Sato et al., 2009, 2011b).

IL10RB knockout causes Paneth cell deficiency in hSIOs

Mutations in the IL-22 co-receptor gene *IL10RB* cause rare, hereditary forms of IBD (Begue et al., 2011; Glocker et al., 2009). We created two such loss-of-function mutations of *IL10RB* (W159* and W204*) using CRISPR-mediated base editing (Figure S5D). As expected, hSIOs carrying either of these two mutations lacked Paneth cells when maintained in maturation medium + IL-22, whereas the frequency of goblet cells and EECs remained unaffected in these mutants (Figures 5A, 5B, and 5E). The requirement of IL10RB for IL-22-induced Paneth cell formation was further confirmed by immunohistochemistry staining of lysozyme (Figures 5C and 5D). IL10RB is a component of the receptors for several interleukins including IL-10, IL-22, IL-26, IL-28A, IL-28B, and IL-29. Although defective IL10 signaling has been considered as the main pathogenic factor in *IL10RB*-deficient IBD, additive or synergistic effects of other signaling pathways are not excluded (Begue et al., 2011; Glocker et al., 2009). In particular, it has been shown that defective IL-22 signaling due to the absence of IL10RB (but not IL10RA) may additionally impair intestinal epithelial bacterial clearance (Begue et al., 2011).

PI3K/AKT/mTOR axis mediates human Paneth cell differentiation downstream of IL-22

To understand the mechanism of IL-22-induced Paneth cell differentiation, we examined the IL-22 downstream signaling pathways, STAT3 and PI3K/AKT/mammalian target of rapamycin (mTOR), by small-molecule inhibitors. In organoids cultured with maturation medium (+IL-22), blocking of STAT3 activation by BP-1-102 had no effect on the proportion of DEFA5-positive Paneth cells compared with untreated organoids (Figures 6A and 6B, S6D–H). In contrast, inhibitors of either PI3K (LY294002) or

AKT (MK-2206) significantly reduced the frequency of Paneth cells (Figures 6A and 6B). More remarkably, mTOR inhibition almost completely blocked IL-22-induced Paneth cell differentiation (Figures 6A, 6B, and S6D–S6H). The PI3K, AKT, or mTOR inhibitors reduced Paneth cell frequency in a dose-dependent manner without significant alteration in the frequency of goblet cells (Figures S6A–S6C). These results implied that the PI3K/AKT/mTOR signaling axis specifically drives Paneth cell differentiation without affecting the other secretory lineages (Figure 6D).

We further conducted quantitative proteome profiling of maturation medium-cultured organoids under four different conditions: –IL-22, +IL-22, +IL-22 with STAT3 inhibitor (BP-1-102), and +IL-22 with mTOR inhibitor (rapamycin). IL-22 strongly upregulated several Paneth cell proteins including DEFA5, DEFA6, REG3A, and ITLN2 (Figure 6C). The increase in these proteins was impaired upon inhibition of mTOR (but not of STAT3) (Figure 6C). These data provided further evidence at the proteome level that mTOR mediates Paneth cell differentiation downstream of IL-22 (Figure 6D).

IL-22-induced expression of AMPs are not restricted to Paneth cells

Pseudobulk differential expression analysis of scRNA-seq data revealed the IL-22-mediated induction of a set of genes related to host defense (Figures 2D and S7A and Table S3), supporting an important role of IL-22 in this process (Forbester et al., 2018; Sanos et al., 2009; Sonnenberg et al., 2011; Zhang et al., 2020). With the exception of some Paneth cell-specific genes (such as DEFA6 and ITLN2), the top-50 IL-22 upregulated genes were expressed across all cell types (Figures 7A and 7B). These genes included AMPs (REG1A, REG1B, and DMBT1), complement factors (such as CFI), and mucins (such as MUC1) (Figure 7B). Indeed, the IL-22 co-receptors IL10RB and IL22RA were expressed by all epithelial cell types in hSIOs (Figure S7B). The expression of these genes (such as REG1A, REG1B, and DMBT1) was significantly induced by IL-22 stimulation within 24 h (Figure 7C). The expression of these AMP genes was not driven by the same signaling pathway as Paneth cell differentiation because the expression of these genes, unlike Paneth cell markers, was not affected by rapamycin treatment (Figure S7C and Table S4).

Histological analysis of three of the top genes that are not restricted to Paneth cells (REG1A, REG1B, and DMBT1) on human small intestinal sections revealed that their expression was highest in the bottom half of crypts (Figure 7D, Human Protein Atlas; Uhlen et al., 2015). It has been established that IL-22 is constitutively expressed in both mouse and human small intestine in which IL-22 is produced by lymphocytes (Sabat et al., 2014). Collectively, these data indicate that IL-22 might serve as a niche factor for host defense at the crypt

Data are shown as mean ± SEM. ns, not significant, multiple t tests using two-stage linear step-up procedure of Benjamini, Krieger, and Yekutieli, with Q = 5%, n = 3.

(F) Cell death as determined by FACS analysis of propidium iodide positive cells.

Data are shown as mean ± SEM. *p < 0.05; multiple t tests using two-stage linear step-up procedure of Benjamini, Krieger, and Yekutieli, with Q = 5%, n = 3.

(G) Stacked bar plot showing the comparison of the early enterocyte and enterocyte cell cluster proportions identified in the integrative scRNA-seq datasets from maturation medium-cultured organoids with or without IL-22.

(H) Stacked bar plot showing the comparison of enterocyte-related gene expression (ANPEP, CYP3A4) in different cell clusters identified in the integrative scRNA-seq datasets from maturation medium-cultured organoids with or without the addition of IL-22. See also Figure S1.

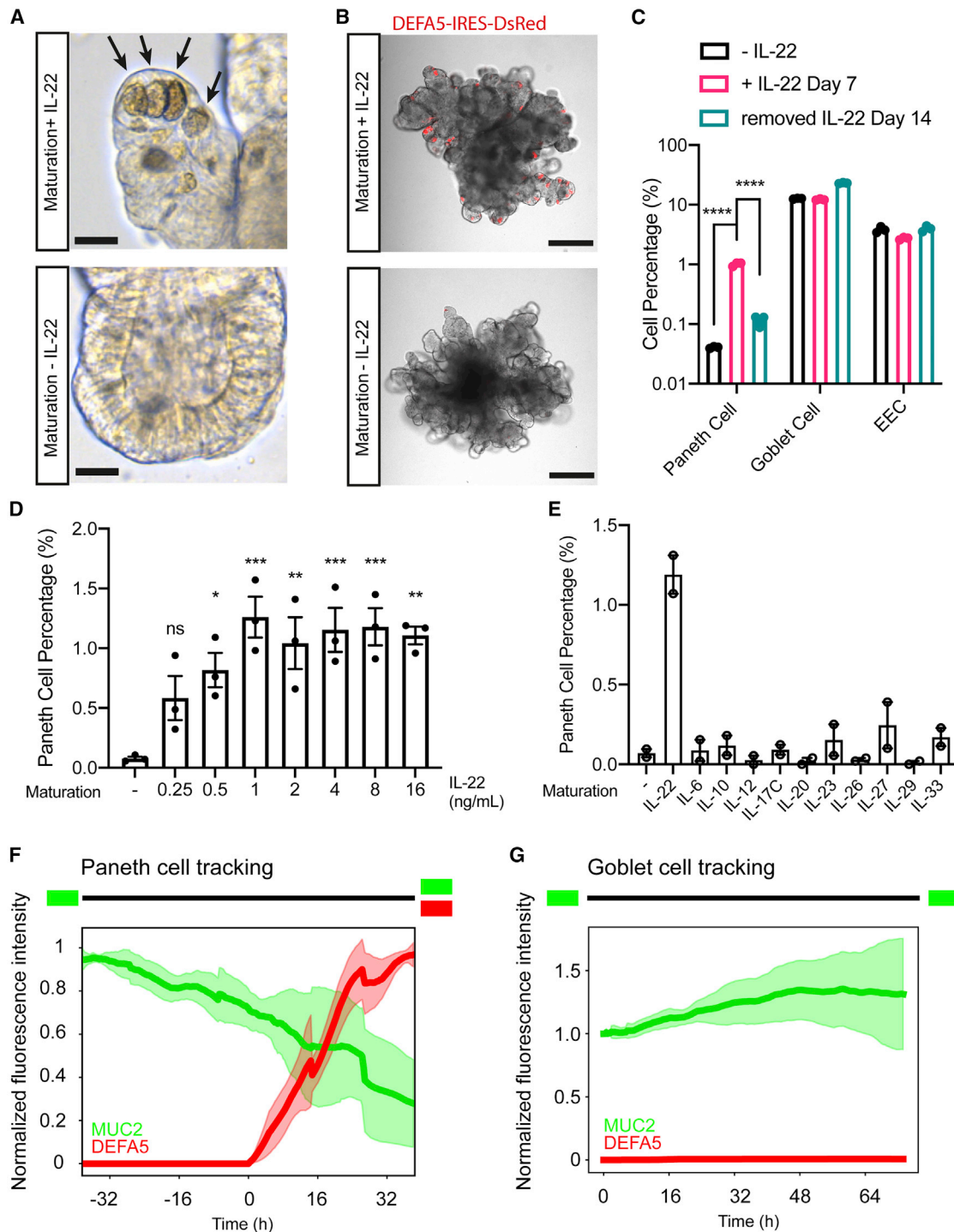


Figure 4. IL-22 induces differentiation of human Paneth cells

(A) Representative image of budding crypts of maturation medium-cultured organoids with or without the addition of IL-22 for 14 days. The black arrowheads highlight the Paneth cells located at the crypt bottom. Scale bars, 20 μ m.

(B) Representative confocal images of maturation medium-cultured organoids with or without adding IL-22. Scale bars, 200 μ m. Representative marker genes for Paneth (DEFA5, red) cells are highlighted by fluorescent reporters.

(C) Proportions of secretory lineages (Paneth cell, goblet cell, and EEC) as determined by FACS analysis in maturation medium-cultured (+IL-22) organoids without, with or upon withdrawal of IL-22.

Data are shown as mean \pm SEM. **** p < 0.0001; one-way ANOVA compared with maturation medium (+IL-22), n = 3 for each condition.

(legend continued on next page)

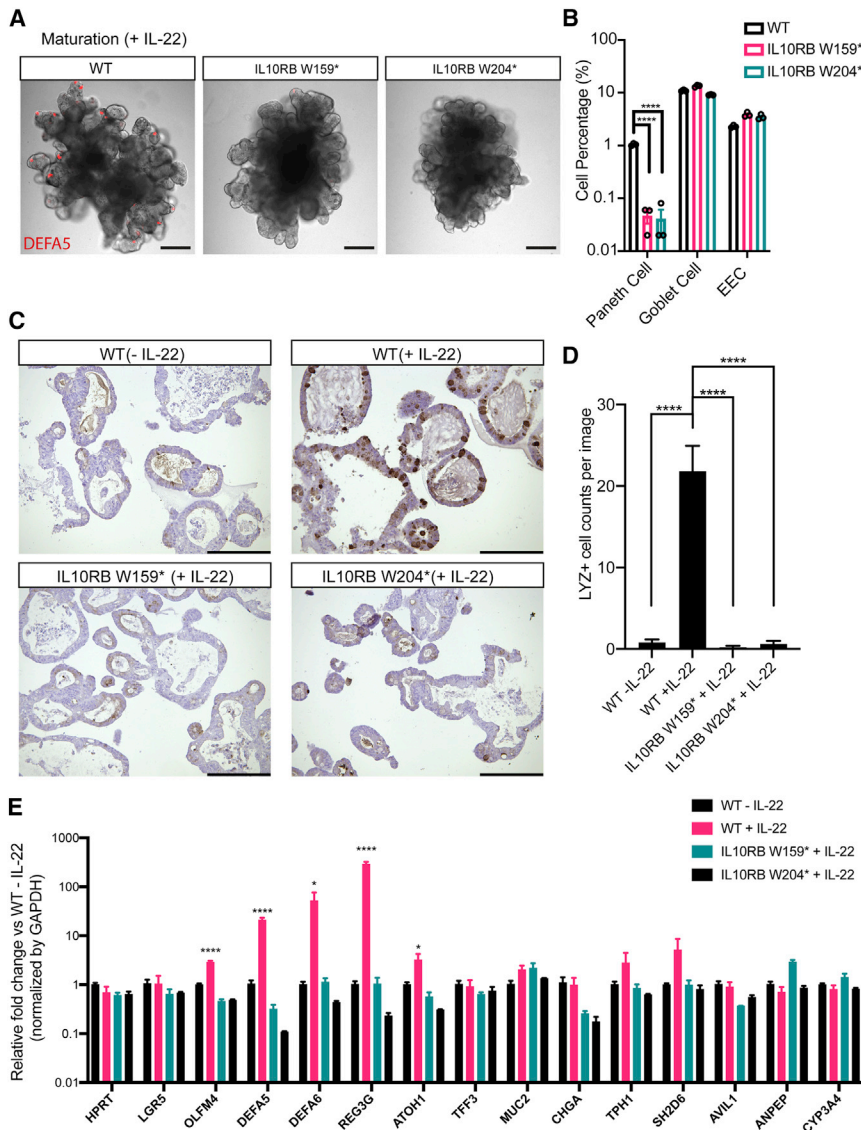


Figure 5. IL10RB is required for IL-22-induced Paneth cell differentiation

(A) Representative confocal image of maturation medium-cultured (+IL-22) organoids with wild-type (WT) genotype or IL10RB variants for 14 days. Scale bars, 200 μ m. Representative marker genes for Paneth (DEFA5, red), enteroendocrine (CHGA, magenta), and goblet (MUC2, green) cells are highlighted by fluorescent reporters.

(B) Proportions of secretory lineages (Paneth cell, goblet cell, and EEC) as determined by FACS analysis in maturation medium-cultured (+IL-22) organoids with WT genotype or IL10RB variants for 7 days.

Data are shown as mean \pm SEM. **** p < 0.0001; one-way ANOVA compared with WT, n = 3 for each line.

(C) Representative images of immunohistochemistry staining of LYZ. Scale bars, 125 μ m.

(D) Quantification of LYZ-positive cells per image. Data are shown as mean \pm SEM. **** p < 0.0001; one-way ANOVA compared with maturation medium (+IL-22), n = 5 for each condition.

(E) RT-qPCR quantification of cell markers expression.

Data are shown as mean \pm SEM. * p < 0.05, ** p < 0.01, *** p < 0.001; one-way ANOVA compared with maturation medium-cultured organoids (-IL-22), n = 3 for each treatment. See also Figure S5.

base in which IL-22 induces not only Paneth cell differentiation, but also the expression of AMPs in intestinal stem cells and their daughters.

DISCUSSION

Here, we describe the establishment of an optimized culturing system for hSIOs. In contrast to existing protocols developed

by us and others (Fuji et al., 2018; Jarde et al., 2020; Pleguezuelos-Manzano et al., 2020), this protocol allows the formation of extensive budding structures with mature Paneth cells, recapitulating human intestinal crypts *in vitro*. By probing the direct effects of IL-22 on the induction of the various epithelial cell types of the human small intestinal epithelium, our study demonstrates that the optimized culture condition markedly im-

proves *ex vivo* modeling of the human intestinal epithelium and significantly broadens the application of human intestinal organoids.

A previous study has claimed that IL-22 promotes intestinal stem cell activity *in vitro* and, consequently, epithelial regeneration (Lindemans et al., 2015). This study used (amongst others) surface area as a measure of growth of organoids. We observe that IL-22 induces swelling of organoids but leads to a decrease in absolute

(D) Proportion of Paneth cells as determined by FACS analysis of DEFA5 reporter in maturation medium-cultured organoids with addition of different dosages of IL-22 for 7 days.

Data are shown as mean \pm SEM. ns, not significant, * p < 0.05, ** p < 0.01, *** p < 0.001; one-way ANOVA compared with maturation medium (-IL-22), n = 3 for each condition.

(E) Proportion of Paneth cells as determined by FACS analysis of DEFA5 reporter in maturation medium-cultured organoids in response to different cytokines for 7 days.

Data are shown as mean \pm SEM, n = 2. IL-22 (2 ng/mL); IL-6 (10 ng/mL); IL-10 (10 ng/mL); IL-12 (10 ng/mL); IL-17C (10 ng/mL); IL-20 (10 ng/mL); IL-23 (10 ng/mL); IL-26 (10 ng/mL); IL-27 (10 ng/mL); IL-29 (10 ng/mL); IL-33 (10 ng/mL).

(F and G) Live imaging tracking Paneth cell and goblet cell reporter signals, an average with standard error (shadow area) of normalized fluorescence intensity from 3 organoids, 8 Paneth cells (F), and 7 goblet cells (G). 0 h in (F): Appearance of DEFA5 signals; 0 h in (G): starting timepoint of tracking. See also Figure S5.

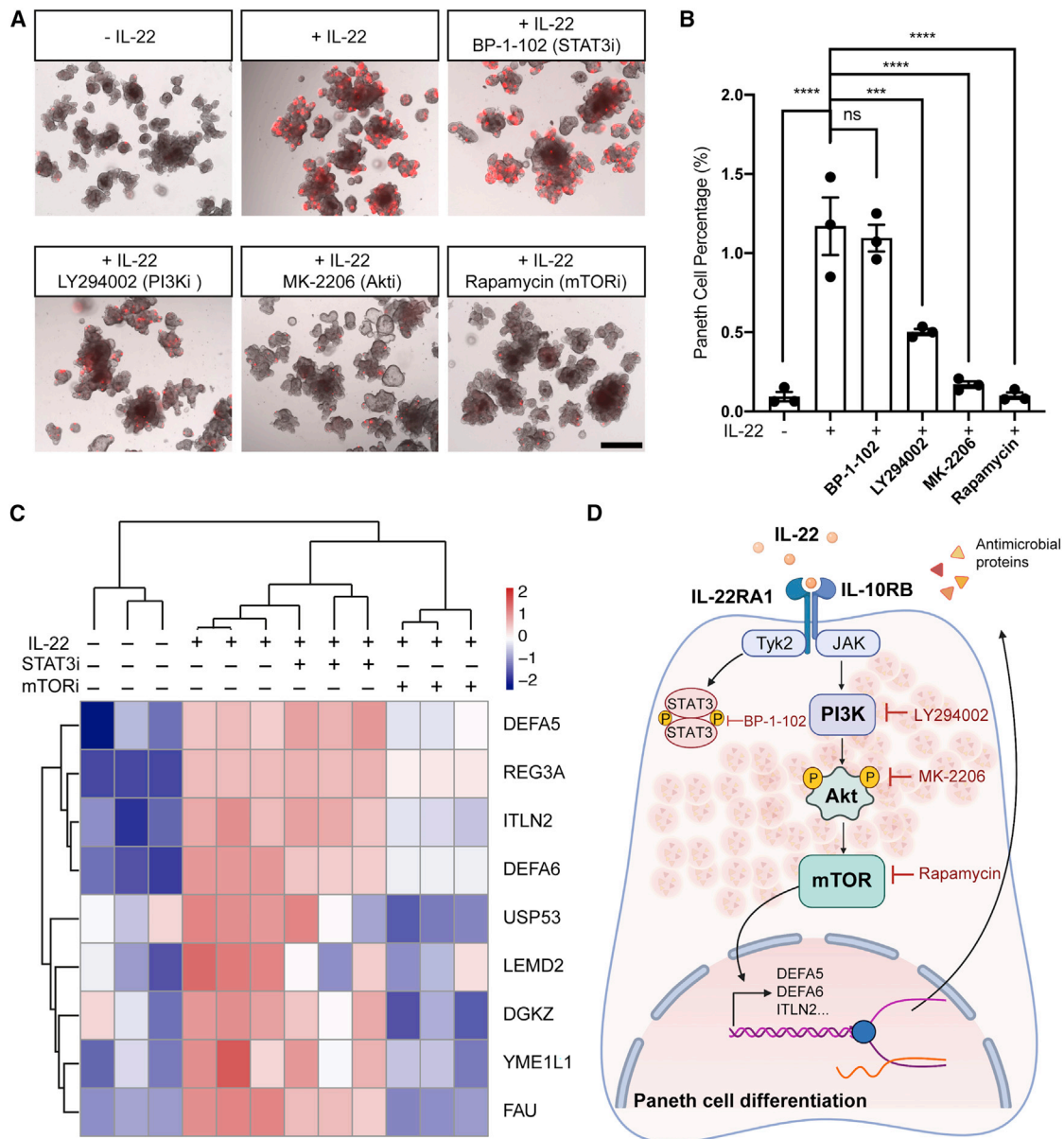


Figure 6. PI3K-mTOR signaling mediates Paneth cell differentiation downstream of IL-22

(A) Representative images of maturation medium-cultured organoids with different treatments described in the legends for 7 days. Scale bars, 500 μ m. The treatments include the presence (+) or absence (-) of IL-22 (2 ng/mL). Small molecules BP-1-102 (5 μ M), LY294002 (1 μ M), MK-2206 (100 nM), and rapamycin (100 nM) were added to the organoids in combination with IL-22 (2 ng/mL).

(B) Proportions of Paneth cells as determined by FACS analysis in maturation medium-cultured organoids by DEFA5-IRES-DsRed reporter with different treatments for 7 days.

Data are shown as mean \pm SEM. ns, not significant, ***p < 0.001, ****p < 0.0001; one-way ANOVA compared with maturation medium culture (+IL-22), n = 3 for each treatment.

(C) Heat map representation of the proteins upregulated by IL-22 treatment for 3 days but reversed by rapamycin. Scale represents scaled protein abundance and ranges from low (blue) to high (red).

(D) Schematics of IL-22 signaling in regulating human Paneth cell differentiation. Small molecule inhibitors targeting different signaling components are highlighted in red. See also Figure S6.

cell numbers. Also, the previous study interpreted the relative ratio of ISCs as an indication of stem cell expansion. We confirmed that IL-22 increases the relative ratio of ISCs in both mouse and human organoids but find that the absolute number of ISCs remains unchanged. This, we find, is a consequence of IL-22 in preventing

ISC differentiation into the normally abundant enterocytes, challenging the notion of activating IL-22 signaling to induce epithelial regeneration for the treatment of intestinal diseases.

Taking advantage of this optimized hSIO model, we find that IL-22 drives human Paneth cells differentiation. Of note, IL-22

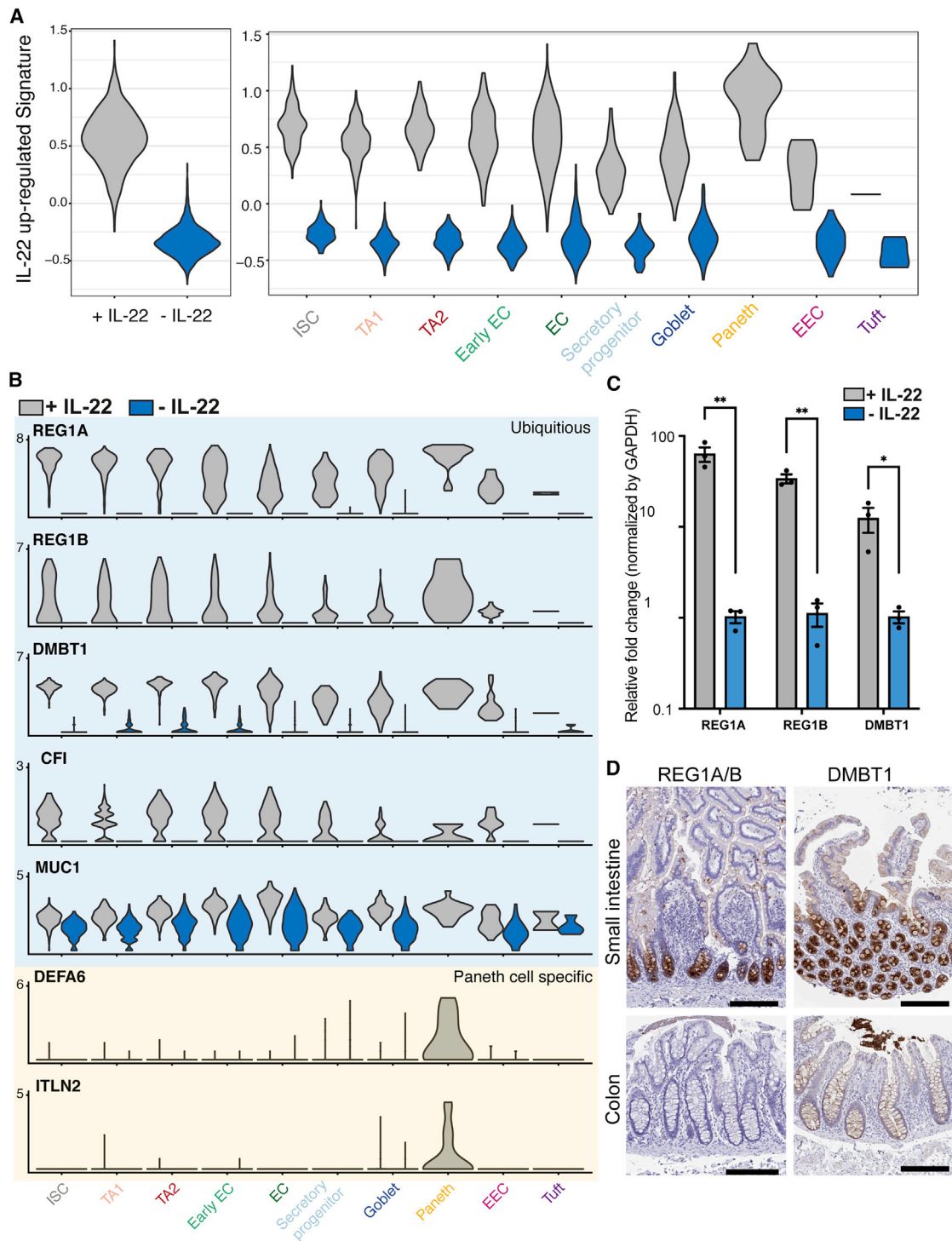


Figure 7. IL-22 induces host defense gene expression

(A) Violin plots of IL22-induced module score in maturation medium-cultured organoids with or without IL-22 (left, average; right, split by cluster).

(B) Stacked bar plots showing the ubiquitous upregulation of gene expression levels of REG1A, REG1B, DMBT1, CFI, and MUC1, the Paneth-specific induction of gene expression levels of DEFA6 and ITLN2, split by cell clusters, in maturation medium-cultured organoids with or without IL-22 by scRNA-seq.

(C) RT-qPCR quantification of REG1A, REG1B, and DMBT1 expression in maturation medium-cultured organoids in response to IL-22 treatment after 24 h. Data are shown as mean \pm SEM. * $p < 0.05$, ** $p < 0.01$, *** $p < 0.001$; multiple t tests using two-stage linear step-up procedure of Benjamini, Krieger, and Yekutieli, with $Q = 5\%$, $n = 3$.

(D) Immunohistochemistry staining of REG1A/B (left: HPA045579, Human Protein Atlas) and DMBT1 (right: HPA040778, Human Protein Atlas) in human small intestine and colon. Scale bars, 200 μm . See also [Figure S7](#).

is not required for the formation of Paneth cells in mouse SIO culture (Lindemans et al., 2015; Sato et al., 2009, 2011b), indicating a fundamental difference between human and mouse in Paneth cells differentiation. Our results further demonstrate that the PI3K/AKT/mTOR signaling axis is essential for IL-22-induced human Paneth cell formation. Two previous studies have reported that IL-22- or intestinal IL-22Ra1- knockout mice display Paneth cell defects via STAT3 signaling (Chiang et al., 2022; Gaudino et al., 2021). Interestingly, Paneth cell-restricted deficiency in raptor or mTOR resulted in nearly complete disappearance of these cells in naive mice, indicating that Paneth cells require intrinsic mTORC1 signaling (Araujo et al., 2021). However, another study shows that TSC2 inactivation results in altered Paneth cell differentiation, which could be rescued by rapamycin (Zhou et al., 2015). Additional work will be required to reconcile these seemingly contradictory findings in mice. Finally, the mTORC1 pathway in Paneth cells plays an important role in sensing the metabolic state of crypts and in the subsequent regulation of stem cell function (Yilmaz et al., 2012). Given that Paneth cells are the main producer of human intestinal AMPs and that their defects have been implicated in the pathogenesis of human intestinal diseases such as infection and IBD (Bevins and Salzman, 2011; Clevers and Bevins, 2013), the discovery of IL-22 signaling in Paneth cell formation may provide a potential therapeutic avenue for these diseases.

In summary, we have developed an optimized organoid culture system to model human intestinal physiology and pathophysiology. Using this model, we identify an essential role for IL-22 in the induction of human Paneth cell differentiation program through the PI3K/AKT/mTOR axis.

Limitations of the study

Optimized hSIOs recapitulate the cellular diversity of human intestinal crypts but do not recapitulate the maturation of villus epithelial cells that are driven by a bone morphogenetic protein (BMP) gradient (high at the villus tip *in vivo*) and countering a Wnt gradient (high at the crypt base *in vivo*). It is expected that establishing these two gradients *in vitro* in organoids will require bio-engineering approaches and will further the development of genuine crypt-to-villus structures *in vitro*.

In addition, we identify IL-22 as an inducer of Paneth cell formation in optimized hSIOs *in vitro* in the context of a high Wnt signaling environment. Current experiments do not prove that IL-22 is the sole, essential inducer of Paneth cell formation *in vivo*.

STAR★METHODS

Detailed methods are provided in the online version of this paper and include the following:

- KEY RESOURCES TABLE
- RESOURCE AVAILABILITY
 - Lead contact
 - Materials availability
 - Data and code availability
- EXPERIMENTAL MODEL AND SUBJECT DETAILS
- METHOD DETAILS

- Organoid culture and drug stimulation
- CRISPR engineering of human intestinal organoids
- Clone formation assay
- EdU cell proliferation assay
- Cell death assay
- RNA extraction and real-time PCR analysis
- Flow cytometry
- Western blot
- Transmission electron microscopy
- Immunohistochemistry staining
- Confocal imaging
- Time-lapse imaging
- Single-cell tracking and the quantification of fluorescence signal
- Single-cell transcriptome sample preparation
- Proteome sample preparation
- LC-MS/MS analyses
- QUANTIFICATION AND STATISTICAL ANALYSIS
 - Single-cell RNA-sequencing data processing

SUPPLEMENTAL INFORMATION

Supplemental information can be found online at <https://doi.org/10.1016/j.stem.2022.08.002>.

ACKNOWLEDGMENTS

We thank Stieneke van den Brink for RSP01-conditioned medium production, Jeroen Korving for histological staining support, Reinier van der Linden for FACS support, Dr. Kai Kretzschmar for generating the original wild-type human intestinal organoid line, and Drs. Joep Beumer and Deliah Hendriks for providing the MUC2 reporter line. Illustrative diagrams were created with BioRender.com.

This publication is part of the project Organoid in time with project number 2019.085 of the research program NWO Investment Large, which is financed by the Dutch Research Council (NWO) and the NWO building blocks of life project, cell dynamics within lung and intestinal organoids (737.016.009), by the Netherlands Organ-on-Chip Initiative, an NWO Gravitation project (024.003.001) funded by the Ministry of Education, Culture and Science of the government of the Netherlands. Supported by the European Union's Horizon 2020 research and innovation program INTENS (668294).

AUTHOR CONTRIBUTIONS

G.-W.H., L.L., and H.C. conceptualized the project, interpreted the results, and wrote the manuscript. G.-W.H. and L.L. designed and performed major experiments and analyzed data. J.D., T.M., F.H., and E.B. performed the scRNA-seq experiments and analysis. N.S. and W.W. performed the proteomic experiments and analysis. X.Z., J.v.Z., and S.T. performed imaging-based tracking experiments and analysis. C.L.-I., W.J.v.d.W., and P.J.P. performed transmission electron microscopy. H.B. performed immunohistochemistry staining. T.D. isolated and provided human intestinal organoid lines from additional donors. D.K. and C.K. provided human samples.

DECLARATION OF INTERESTS

H.C. is an inventor of several patents related to organoid technology; his full disclosure is given at <https://www.uu.nl/staff/JCClevers/>.

Received: February 11, 2022

Revised: July 1, 2022

Accepted: August 5, 2022

Published: August 23, 2022; corrected online: November 17, 2022

REFERENCES

- Angerer, P., Haghverdi, L., Büttner, M., Theis, F.J., Marr, C., and Buettner, F. (2016). Destiny: diffusion maps for large-scale single-cell data in R. *Bioinformatics* 32, 1241–1243.
- Araujo, A., Safronova, A., Burger, E., López-Yglesias, A., Giri, S., Camanzo, E.T., Martin, A.T., Grivennikov, S., and Yarovinsky, F. (2021). IFN-gamma mediates paneth cell death via suppression of mTOR. *Elife* 10, e60478.
- Arbab, M., Srinivasan, S., Hashimoto, T., Geijsen, N., and Sherwood, R.I. (2015). Cloning-free CRISPR. *Stem Cell Rep.* 5, 908–917.
- Artegiani, B., Hendriks, D., Beumer, J., Kok, R., Zheng, X., Joore, I., Chuva de Sousa Lopes, S., van Zon, J., Tans, S., and Clevers, H. (2020). Fast and efficient generation of knock-in human organoids using homology-independent CRISPR-Cas9 precision genome editing. *Nat. Cell Biol.* 22, 321–331.
- Begue, B., Verdier, J., Rieux-Laucat, F., Goulet, O., Morali, A., Canioni, D., Hugot, J.P., Daussy, C., Verkarre, V., Pigneur, B., et al. (2011). Defective IL10 signaling defining a subgroup of patients with inflammatory bowel disease. *Am. J. Gastroenterol.* 106, 1544–1555.
- Bergen, V., Lange, M., Peidli, S., Wolf, F.A., and Theis, F.J. (2020). Generalizing RNA velocity to transient cell states through dynamical modeling. *Nat. Biotechnol.* 38, 1408–1414.
- Beumer, J., Puschhof, J., Bauzá-Martinez, J., Martínez-Silgado, A., Elmentaite, R., James, K.R., Ross, A., Hendriks, D., Artegiani, B., Busslinger, G.A., et al. (2020). High-resolution mRNA and secretome atlas of human enteroendocrine cells. *Cell* 182, 1062–1064.
- Bevins, C.L., and Salzman, N.H. (2011). Paneth cells, antimicrobial peptides and maintenance of intestinal homeostasis. *Nat. Rev. Microbiol.* 9, 356–368.
- Burclaff, J., Bliton, R.J., Breaux, K.A., Ok, M.T., Gomez-Martinez, I., Ranek, J.S., Bhatt, A.P., Purvis, J.E., Woosley, J.T., and Magness, S.T. (2022). A proximal-to-distal survey of healthy adult human small intestine and colon epithelium by single-cell transcriptomics. *Cell. Mol. Gastroenterol. Hepatol.* 13, 1554–1589.
- Busslinger, G.A., Weusten, B.L.A., Bogte, A., Begthel, H., Brosens, L.A.A., and Clevers, H. (2021). Human gastrointestinal epithelia of the esophagus, stomach, and duodenum resolved at single-cell resolution. *Cell Rep.* 34, 108819.
- Chiang, H.Y., Lu, H.H., Sudhakar, J.N., Chen, Y.W., Shih, N.S., Weng, Y.T., and Shui, J.W. (2022). IL-22 initiates an IL-18-dependent epithelial response circuit to enforce intestinal host defence. *Nat. Commun.* 13, 874.
- Clevers, H.C., and Bevins, C.L. (2013). Paneth cells: maestros of the small intestinal crypts. *Annu. Rev. Physiol.* 75, 289–311.
- Cox, J.H., Kljavin, N.M., Ota, N., Leonard, J., Roose-Girma, M., Diehl, L., Ouyang, W., and Ghilardi, N. (2012). Opposing consequences of IL-23 signaling mediated by innate and adaptive cells in chemically induced colitis in mice. *Mucosal Immunol.* 5, 99–109.
- Eken, A., Singh, A.K., Treuting, P.M., and Oukka, M. (2014). IL-23R+ innate lymphoid cells induce colitis via interleukin-22-dependent mechanism. *Mucosal Immunol.* 7, 143–154.
- Forbester, J.L., Lees, E.A., Goulding, D., Forrest, S., Yeung, A., Speak, A., Clare, S., Coomber, E.L., Mukhopadhyay, S., Kraiczy, J., et al. (2018). Interleukin-22 promotes phagolysosomal fusion to induce protection against *Salmonella enterica* Typhimurium in human epithelial cells. *Proc. Natl. Acad. Sci. USA.* 115, 10118–10123.
- Fujii, M., Matano, M., Nanki, K., and Sato, T. (2015). Efficient genetic engineering of human intestinal organoids using electroporation. *Nat. Protoc.* 10, 1474–1485.
- Fujii, M., Matano, M., Toshimitsu, K., Takano, A., Mikami, Y., Nishikori, S., Sugimoto, S., and Sato, T. (2018). Human intestinal organoids maintain self-renewal capacity and cellular diversity in niche-inspired culture condition. *Cell Stem Cell* 23, 787–793.e6.
- Gaudino, S.J., Beaupre, M., Lin, X., Joshi, P., Rathi, S., McLaughlin, P.A., Kempen, C., Mehta, N., Eskiocak, O., Yueh, B., et al. (2021). IL-22 receptor signaling in Paneth cells is critical for their maturation, microbiota colonization, Th17-related immune responses, and anti-Salmonella immunity. *Mucosal Immunol.* 14, 389–401.
- Glocker, E.O., Kotlarz, D., Boztug, K., Gertz, E.M., Schäffer, A.A., Noyan, F., Perro, M., Diestelhorst, J., Allroth, A., Murugan, D., et al. (2009). Inflammatory bowel disease and mutations affecting the interleukin-10 receptor. *N. Engl. J. Med.* 361, 2033–2045.
- Hafemeister, C., and Satija, R. (2019). Normalization and variance stabilization of single-cell RNA-seq data using regularized negative binomial regression. *Genome Biol.* 20, 296.
- Hasegawa, M., Yada, S., Liu, M.Z., Kamada, N., Muñoz-Planillo, R., Do, N., Núñez, G., and Inohara, N. (2014). Interleukin-22 regulates the complement system to promote resistance against pathobionts after pathogen-induced intestinal damage. *Immunity* 41, 620–632.
- Jardé, T., Chan, W.H., Rossello, F.J., Kaur Kahlon, T., Theocharous, M., Kurian Arackal, T., Flores, T., Giraud, M., Richards, E., Chan, E., et al. (2020). Mesenchymal Niche-Derived Neuregulin-1 Drives Intestinal Stem Cell Proliferation and Regeneration of Damaged Epithelium. *Cell Stem Cell* 27, 646–662.e7.
- Keir, M., Yi, T., Lu, T., and Ghilardi, N. (2020). The role of IL-22 in intestinal health and disease. *J. Exp. Med.* 217, e20192195.
- Koblan, L.W., Doman, J.L., Wilson, C., Levy, J.M., Tay, T., Newby, G.A., Maiani, J.P., Raguram, A., and Liu, D.R. (2018). Improving cytidine and adenine base editors by expression optimization and ancestral reconstruction. *Nat. Biotechnol.* 36, 843–846.
- Kok, R.N.U., Hebert, L., Huelsz-Prince, G., Goos, Y.J., Zheng, X., Bozek, K., Stephens, G.J., Tans, S.J., and van Zon, J.S. (2020). OrganoidTracker: Efficient cell tracking using machine learning and manual error correction. *PLoS One* 15, e0240802.
- Layunta, E., Jäverfelt, S., Dolan, B., Arike, L., and Pelaseyed, T. (2021). IL-22 promotes the formation of a MUC17 glycocalyx barrier in the postnatal small intestine during weaning. *Cell Rep.* 34, 108757.
- Lindemans, C.A., Calafiore, M., Mertelsmann, A.M., O'Connor, M.H., Dudakov, J.A., Jenq, R.R., Velardi, E., Young, L.F., Smith, O.M., Lawrence, G., et al. (2015). Interleukin-22 promotes intestinal-stem-cell-mediated epithelial regeneration. *Nature* 528, 560–564.
- Mizoguchi, A., Yano, A., Himuro, H., Ezaki, Y., Sadanaga, T., and Mizoguchi, E. (2018). Clinical importance of IL-22 cascade in IBD. *J. Gastroenterol.* 53, 465–474.
- Pelczar, P., Witkowski, M., Perez, L.G., Kempski, J., Hammel, A.G., Brockmann, L., Kleinschmidt, D., Wende, S., Haueis, C., Bedke, T., et al. (2016). A pathogenic role for T cell-derived IL-22BP in inflammatory bowel disease. *Science* 354, 358–362.
- Pleguezuelos-Manzano, C., Puschhof, J., van den Brink, S., Geurts, V., Beumer, J., and Clevers, H. (2020). Establishment and culture of human intestinal organoids derived from adult stem cells. *Curr. Protoc. Immunol.* 130, e106.
- Reyes, J.L., Fernando, M.R., Lopes, F., Leung, G., Mancini, N.L., Matisz, C.E., Wang, A., and McKay, D.M. (2016). IL-22 restrains tapeworm-mediated protection against experimental colitis via regulation of IL-25 expression. *PLoS Pathog.* 12, e1005481.
- Rothenberg, M.E., Wang, Y., Lekkerkerker, A., Danilenko, D.M., Maciuga, R., Erickson, R., Herman, A., Stefanich, E., and Lu, T.T. (2019). Randomized phase I healthy volunteer study of UTTR1147A (IL-22Fc): a potential therapy for epithelial injury. *Clin. Pharmacol. Ther.* 105, 177–189.
- Sabat, R., Ouyang, W., and Wolk, K. (2014). Therapeutic opportunities of the IL-22-IL-22R1 system. *Nat. Rev. Drug Discov.* 13, 21–38.
- Sanos, S.L., Bui, V.L., Mortha, A., Oberle, K., Heners, C., Johner, C., and Diefenbach, A. (2009). ROR γ and commensal microflora are required for the differentiation of mucosal interleukin 22-producing NKp46+ cells. *Nat. Immunol.* 10, 83–91.
- Sato, T., Stange, D.E., Ferrante, M., Vries, R.G.J., Van Es, J.H., Van den Brink, S., Van Houdt, W.J., Pronk, A., Van Gorp, J., Siersema, P.D., and Clevers, H. (2011a). Long-term expansion of epithelial organoids from human colon, adenoma, adenocarcinoma, and Barrett's epithelium. *Gastroenterology* 141, 1762–1772.

- Sato, T., van Es, J.H., Snippert, H.J., Stange, D.E., Vries, R.G., van den Born, M., Barker, N., Shroyer, N.F., van de Wetering, M., and Clevers, H. (2011b). Paneth cells constitute the niche for Lgr5 stem cells in intestinal crypts. *Nature* 469, 415–418.
- Sato, T., Vries, R.G., Snippert, H.J., van de Wetering, M., Barker, N., Stange, D.E., van Es, J.H., Abo, A., Kujala, P., Peters, P.J., and Clevers, H. (2009). Single Lgr5 stem cells build crypt-villus structures *in vitro* without a mesenchymal niche. *Nature* 459, 262–265.
- Schmechel, S., Konrad, A., Diegelmann, J., Glas, J., Wetzke, M., Paschos, E., Lohse, P., Göke, B., and Brand, S. (2008). Linking genetic susceptibility to Crohn's disease with Th17 cell function: IL-22 serum levels are increased in Crohn's disease and correlate with disease activity and IL23R genotype status. *Inflamm. Bowel Dis.* 14, 204–212.
- Sonnenberg, G.F., Fouser, L.A., and Artis, D. (2011). Border patrol: regulation of immunity, inflammation and tissue homeostasis at barrier surfaces by IL-22. *Nat. Immunol.* 12, 383–390.
- Stefanich, E.G., Rae, J., Sukumaran, S., Lutman, J., Lekkerkerker, A., Ouyang, W., Wang, X., Lee, D., Danilenko, D.M., Diehl, L., et al. (2018). Pre-clinical and translational pharmacology of a human interleukin-22 IgG fusion protein for potential treatment of infectious or inflammatory diseases. *Biochem. Pharmacol.* 152, 224–235.
- Street, K., Risso, D., Fletcher, R.B., Das, D., Ngai, J., Yosef, N., Purdom, E., and Dudoit, S. (2018). Slingshot: cell lineage and pseudotime inference for single-cell transcriptomics. *BMC Genom.* 19, 477.
- Stuart, T., Butler, A., Hoffman, P., Hafemeister, C., Papalexi, E., Mauck, W.M., 3rd, Hao, Y., Stoeckius, M., Smibert, P., and Satija, R. (2019). Comprehensive Integration of Single-Cell Data. *Cell* 177, 1888–1902.e21.
- Sugimoto, K., Ogawa, A., Mizoguchi, E., Shimomura, Y., Andoh, A., Bhan, A.K., Blumberg, R.S., Xavier, R.J., and Mizoguchi, A. (2008). IL-22 ameliorates intestinal inflammation in a mouse model of ulcerative colitis. *J. Clin. Invest.* 118, 534–544.
- Tirosh, I., Izar, B., Prakadan, S.M., Wadsworth, M.H., 2nd, Treacy, D., Trombetta, J.J., Rotem, A., Rodman, C., Lian, C., Murphy, G., et al. (2016). Dissecting the multicellular ecosystem of metastatic melanoma by single-cell RNA-seq. *Science* 352, 189–196.
- Turner, J.E., Stockinger, B., and Helmbly, H. (2013). IL-22 mediates goblet cell hyperplasia and worm expulsion in intestinal helminth infection. *PLoS Pathog.* 9, e1003698.
- Uhlén, M., Fagerberg, L., Hallström, B.M., Lindskog, C., Oksvold, P., Mardinoglu, A., Sivertsson, Å., Kampf, C., Sjöstedt, E., Asplund, A., et al. (2015). Proteomics. tissue-based map of the human proteome. *Science* 347, 1260419.
- Yang, Q., Bermingham, N.A., Finegold, M.J., and Zoghbi, H.Y. (2001). Requirement of Math1 for secretory cell lineage commitment in the mouse intestine. *Science* 294, 2155–2158.
- Yilmaz, Ö.H., Katajisto, P., Lamming, D.W., Gültekin, Y., Bauer-Rowe, K.E., Sengupta, S., Birsoy, K., Dursun, A., Yilmaz, V.O., Selig, M., et al. (2012). mTORC1 in the paneth cell niche couples intestinal stem-cell function to calorie intake. *Nature* 486, 490–495.
- Zenewicz, L.A., Yancopoulos, G.D., Valenzuela, D.M., Murphy, A.J., Stevens, S., and Flavell, R.A. (2008). Innate and adaptive interleukin-22 protects mice from inflammatory bowel disease. *Immunity* 29, 947–957.
- Zha, J.M., Li, H.S., Lin, Q., Kuo, W.T., Jiang, Z.H., Tsai, P.Y., Ding, N., Wu, J., Xu, S.F., Wang, Y.T., et al. (2019). Interleukin 22 Expands Transit-Amplifying Cells While Depleting Lgr5(+) Stem cells via inhibition of Wnt and notch signaling. *Cell. Mol. Gastroenterol. Hepatol.* 7, 255–274.
- Zhang, Z., Zou, J., Shi, Z., Zhang, B., Etienne-Mesmin, L., Wang, Y., Shi, X., Shao, F., Chassaing, B., and Gewirtz, A.T. (2020). IL-22-induced cell extrusion and IL-18-induced cell death prevent and cure rotavirus infection. *Sci. Immunol.* 5, eabd2876.
- Zhou, Y., Rychahou, P., Wang, Q., Weiss, H.L., and Evers, B.M. (2015). TSC2/mTORC1 signaling controls Paneth and goblet cell differentiation in the intestinal epithelium. *Cell Death Dis.* 6, e1631.
- Zwarycz, B., Gracz, A.D., Rivera, K.R., Williamson, I.A., Samsa, L.A., Starmer, J., Daniele, M.A., Salter-Cid, L., Zhao, Q., and Magness, S.T. (2019). IL22 inhibits epithelial stem cell expansion in an Ileal organoid model. *Cell. Mol. Gastroenterol. Hepatol.* 7, 1–17.

STAR★METHODS

KEY RESOURCES TABLE

REAGENT or RESOURCE	SOURCE	IDENTIFIER
Chemicals		
Advanced DMEM/F-12	GIBCO	Cat#12634028
Opti-MEM™ I Reduced Serum Medium	GIBCO	Cat#11058021
Penicillin-Streptomycin (10,000 U/mL)	GIBCO	Cat#15140122
HEPES (1M)	GIBCO	Cat#15630056
GlutaMAX™ Supplement	GIBCO	Cat#35050038
Primocin (50 mg/mL)	InvivoGen	Cat#ant-pm-1
B27 Supplement (50X)	ThermoFisher	Cat#12587010
TrypLE™ Express Enzyme (1X), phenol red	ThermoFisher	Cat#12605010
Wnt surrogate-fc fusion protein	U-PROTEIN EXPRESS BV	Cat#N001-0.5mg
Noggin-fc fusion protein conditioned medium	U-PROTEIN EXPRESS BV	Cat#N002 - 100 mL
Animal-Free Recombinant Human EGF	Peprotech	Cat#AF-100-15
A83-01	Tocris	Cat#2939
SB202190	Sigma	Cat# S7067
Prostaglandin E2 10mg	Tocris	Cat#2296
Gastrin I (human) 1 mg	Tocris	Cat#3006
CHIR 99021 10mg	Stemgent	Cat# 04-0004-base
Recombinant Human IL-22	Peprotech	Cat#200-22
Recombinant Murine IL-22	Peprotech	Cat#210-22
N-Acetyl-L-cysteine	Sigma	Cat#A9165
Nicotinamide (1M)	Sigma	Cat#N0636
Recombinant RNasin® RNase Inhibitor, 10,000 U	Promega	Cat#N2515
GoScript™ Reverse Transcriptase kit	Promega	Cat#A5000
Oligo(dT) 15 Primer, 500ug/ml 20ug	Promega	Cat#C1101
Random Primer, 500ug/ml 20ug	Promega	Cat#C1181
Agel-HF	NEB	Cat#R3552L
BbsI-HF	NEB	Cat#R3539S
RNeasy Mini Kit (250)	Qiagen	Cat#74106
BP-1-102	Selleckchem	Cat#S7769
LY294002	Cayman Chemical	Cat#70920
MK-2206 2HCl	Selleckchem	Cat#S1078
Rapamycin (AY-22989)	Selleckchem	Cat#S1039
Y-27632 dihydrochloride	Abmole Bioscience	Cat#M1817
iQ™ SYBR® Green Supermix	BioRad	Cat#1708887
DAPI, 4',6-Diamidino-2'-phenylindole dihydrochloride	Sigma	Cat#10236276001
Click-iT™ Plus EdU Alexa Fluor™ 647 Flow Cytometry Assay Kit	ThermoFisher	Cat#C10634
Antibodies		
Chr-A Antibody (C-20)	Santa Cruz	Cat#sc-1488; RRID:AB_2276319
Lysozyme EC 3.2.1.17	Dako	Cat#A0099; RRID:AB_578661
Phospho-Stat3 (Tyr705) (D3A7) XP® Rabbit mAb	Cell Signaling Technology	Cat#9145T; RRID:AB_2491009
Stat3 (79D7) Rabbit mAb	Cell Signaling Technology	Cat#4904T; RRID:AB_331269
Phospho-Akt (Ser473) Antibody	Cell Signaling Technology	Cat#9271T; RRID:AB_329825
Akt (pan) (11E7) Rabbit mAb	Cell Signaling Technology	Cat#4685S; RRID:AB_2225340
Phospho-S6 Ribosomal Protein (Ser235/236) (D57.2.2E) XP® Rabbit mAb	Cell Signaling Technology	Cat#4858S; RRID:AB_916156

(Continued on next page)

Continued		
REAGENT or RESOURCE	SOURCE	IDENTIFIER
S6 Ribosomal Protein (5G10) Rabbit mAb	Cell Signaling Technology	Cat#2217S; RRID:AB_331355
β-Actin (13E5) Rabbit mAb (HRP Conjugate)	Cell Signaling Technology	Cat#5125S; RRID:AB_1903890
Swine Anti-Rabbit Immunoglobulins/HRP	Dako	Cat#P0217; RRID:AB_2728719
Deposited data		
Proteomics profiling of hSIOs with or without addition of IL-22 and drug treatments	this paper	ProteomeXchange: PXD028746
scRNA-seq profiling of hSIOs with or without addition of IL-22	this paper	GEO:GSE189423
Code required to reproduce the single-cell RNA-sequencing analysis	this paper	https://github.com/jeffdemartino/PanethAnalysis
Recombinant DNA		
sgBbsI (p2Tol-U6-2xBbsI-sgRNA-HygR)	Arbab et al., 2015	Addgene, Cat#71485
spCas9-BlastR (pCBhCas9-BlastR)	Arbab et al., 2015	Addgene, Cat#71489
Software and algorithms		
FlowJo software 10.4	FlowJo	https://www.flowjo.com
ImageJ 1.53	ImageJ	https://imagej.nih.gov/ij/index.html
Prism 8.2.0	GraphPad	https://www.graphpad.com/scientific-software/prism/
Rstudio	Rstudio	https://rstudio.com/
R (v4.1.0)	R	https://www.r-project.org/
Seurat (v4.0.3)	Stuart et al., 2019	https://satijalab.org/seurat/
scVelo python (v0.2.2, python v3.7)	Bergen et al., 2020	https://scvelo.readthedocs.io/
destiny (v3.1.1)	Angerer et al., 2016	https://bioconductor.org/packages/release/bioc/html/destiny.html
Slingshot (v2.0.0)	Street et al., 2018	https://bioconductor.org/packages/release/bioc/html/slingshot.html
Experimental models: Organoid lines		
Donor1: N39	Beumer et al., 2020	HUB
Donor2: NKI1	this paper	NKI-Hubrecht
Donor3: NKI2	this paper	NKI-Hubrecht
Donor4: NKI3	this paper	NKI-Hubrecht
Oligonucleotides		
qPCR primers	this paper	Table S1 Oligo Collection

RESOURCE AVAILABILITY

Lead contact

Further information and requests for resources and reagents should be directed to and will be fulfilled by the lead contact, Hans Clevers (h.clevers@hubrecht.eu).

Materials availability

This study did not generate new unique materials.

Data and code availability

The mass spectrometry (MS)-based proteomics data have been deposited to the ProteomeXchange Consortium via the PRIDE partner repository with the dataset identifier PXD028746. The single-cell RNA-sequencing data have been deposited in the Gene Expression Omnibus (GEO), accession number GSE189423. The accession numbers are listed in the [key resources table](#).

The code required to reproduce the single-cell RNA-sequencing analysis detailed above is available in the github repository <https://github.com/jeffdemartino/PanethAnalysis>. The accession link is listed in the [key resources table](#).

Any additional information required to reanalyze the data reported in this paper is available from the [lead contact](#) upon request.

EXPERIMENTAL MODEL AND SUBJECT DETAILS

Three human small intestine organoid lines established from the ileum tissues of three different donors were used in this study (donor1: N39 (Beumer et al., 2020), male; donor2: NK11, male; donor3: NK12, male). One organoid line derived from the duodenum tissues of one donor was used in this study (donor4: NK13, female). The human organoid line in use (donor1: N39) was derived by intestinal endoscopic biopsy from the ileum, and used in previous studies. The patient's informed consent was obtained, and the study was approved by the ethics committee of the University Medical Center Utrecht. The other human organoid lines in use (donor2: NK11, donor3: NK12, donor4: NK13) were obtained as normal adjacent tissue from tumor resections. The patients' informed consents were obtained, and the study was approved by the ethics committee of the NKI IRB with code CFMPB582. This study is compliant with all relevant ethical regulations regarding research involving human participants.

METHOD DETAILS

Organoid culture and drug stimulation

The compositions of culture media for hSIO are listed in Figure 1B. The concentrations are: R-Spondin conditioned medium (10%), Noggin conditioned medium (2%, U-Protein Express), B27 (1%), n-Acetyl Cysteine (1,25 mM, Sigma), Nicotinamide (10 mM, Sigma), high Wnt (1:1000 Wnt surrogate, U-Protein Express), low Wnt (1:30,000 Wnt surrogate, U-Protein Express), human EGF (50 ng/mL, PeproTech), human IL-22 (2 ng/ml, PeproTech), A83-01 (500 nM, Tocris), p38 inhibitor SB202190 (3 μ M, Sigma), Prostaglandin E2 (10 nM, Tocris), CHIR99021 (3 μ M, Stemgent), Rho kinase inhibitor Y-27632 dihydrochloride (10 μ M, Abmole Bioscience) and Primocin (100 μ g/mL, InvivoGen) supplemented in basic culture medium consisting of Advanced Dulbecco's modified Eagle's medium (DMEM)/F12 with B27, Glutamax, HEPES, penicillin/streptomycin (Thermo Fisher).

Primary human small intestinal crypts were isolated and cultured in conventional expansion medium as described previously (Sato et al., 2011a). Organoids were split once a week and medium was refreshed every three days. For passaging, organoids were removed from the Cultrex Basement Membrane Extract (BME, Growth Factor Reduced, Type 2, R&D Systems), digested with TrypLE (Thermo Fisher) for 2 min into small clumps of cells, washed with ice-cold AdDMEM/F12 (GIBCO) and replated in fresh BME. For differentiation toward enterocytes, expansion-cultured organoids were replated without trypsinization, and the culture medium was changed to conventional differentiation medium for 5 days.

For patterning, conventional expansion-cultured organoids were replated without trypsinization, and the culture medium was changed to patterning medium for 14 days. Afterward, patterned organoids were replated without trypsinization, and the culture medium was changed to Maturation medium (+/– hIL-22) for long-term maintenance. Organoids were passaged in a similar way as mouse small intestinal organoids. In brief, organoids were removed from BME, mechanically dissociated into small fragments using 1 mL pipette tips, then replated in fresh BME. Both patterning and Maturation medium were refreshed every three days.

Primary mouse small intestinal crypts were isolated from Lgr5 reporter mice and cultured in "ENR" medium as described previously (Sato et al., 2009). The compositions of "ENR" medium is identical to the conventional differentiation medium for hSIOs listed in Figure 1B.

Stock solutions for small molecules were prepared according to manufacturer's recommendation. Small molecules: BP-1-102 (Selleckchem), LY294002 (Cayman Chemical), MK-2206 (Tocris) and rapamycin (Tocris) were added to organoid cultures with defined concentrations. The concentrations and durations of treatment are labeled in the figure legends of each set of experiments.

CRISPR engineering of human intestinal organoids

For fluorescent reporter construction, DEFA5-IRES-dsRed and CHGA-IRES-iRFP670 knock-in-IRES sequences were sequentially introduced into the MUC2-mNeonGreen intestinal organoid line as previously published (Artegiani et al., 2020). gRNA design and HDR arms of DEFA5-IRES-dsRed and CHGA-IRES-iRFP670 are listed in Table S1. HDR knock-in constructs are based on the pcDNA3.1(+) plasmid backbone. pcDNA3.1(+) was first digested with MfeI (NEB) and BbsI (NEB) restriction enzymes to remove CMV expression cassette. Knock-in sequence is designed with HDR homolog containing MfeI and EcoRI cutting sites and cloned into pcDNA3.1(+) backbone using NEBuilder HiFi DNA Assembly (NEB) (Arbab et al., 2015). For base editing, gRNAs were designed to target the respective cytosine located at the IL10RB variants W159* and W204*. The mixture of gRNA plasmids, spCas9 plasmids or BE4max base editing plasmids (Koblan et al., 2018), or together with HDR constructs are introduced into the cells using NEPA electroporation system (NEPAGENE) as previously described (Fuji et al., 2015). Organoid clones derived from single cell expansion are picked manually and expanded for genotyping. The gRNA sequences, genotyping primers, reporter HDR donor sequences are listed in Table S1.

Clone formation assay

Organoids were cultured in the presence (+) or absence (–) of IL-22 (labeled as pre-split) for four weeks. The organoids were then digested into single cells, replated in BME (R&D Systems) in 48-well plates and grown in medium in the presence (+) or absence (–) of IL-22 (labeled as post-split). Clones were counted and quantified two weeks after replating. In Figure 3B, + and – indicate the culture condition with or without IL-22, respectively. "Pre-split" and "post-split" indicate the culture conditions used before or after single cell digestion respectively.

EdU cell proliferation assay

Organoids were cultured in the presence (+) or absence (–) of IL-22 for four weeks. 10 μ M of EdU (5-ethynyl-2'-deoxyuridine) was added to organoid culture medium and incubated for two hours. Organoids were then collected and digested with TrypLE (Thermo Fisher) into single cells. Afterward, cell fixation and permeabilization, and EdU detection were performed according to manufacturer's instructions (Thermo Fisher).

Cell death assay

Organoids were cultured in the presence (+) or absence (–) of IL-22 for four weeks prior to cell death assay. Organoid cultures were removed from BME (R&D Systems) by intense pipetting and centrifuged. Dead cells from supernatants were also collected. Organoid pellets were then digested with TrypLE (Thermo Fisher) into single cells, pooled together with collected supernatants and all cells were harvested by centrifugation at 500 g for 5 min. The harvested cells were resuspended in FACS buffer containing 10 μ g/mL of propidium iodide and incubated at room temperature for 15 min in the dark. Cell death, as determined by propidium iodide staining, was then measured by flow cytometry.

RNA extraction and real-time PCR analysis

Organoid cultures subjected to different treatments were collected and washed with PBS. RNA purification was performed with the RNeasy Mini Kit with DNase treatment (Qiagen), following the manufacturer's protocol. RNA was resuspended and quantified with Nanodrop (Thermo Fisher). We used ~1–2 μ g of DNase-treated RNA for each reverse transcription reaction with Oligo(dT)₁₅ Primer or Random Primer and GoScript™ Reverse Transcriptase kit (Promega). Afterward, cDNA was subjected to qPCR using iQ™ SYBR® Green supermix (BioRad) in CFX Connect™ Real-Time PCR machine (BioRad). For gene expression profiling, qPCR was performed with gene-specific qPCR primers. Ct readouts of each gene were first normalized to the housekeeping gene GAPDH (Δ Ct), and the relative expression of individual genes versus the expression levels in control conditions was then calculated with the $2^{-\Delta\Delta Ct}$ method. All qPCR primers are listed in [Table S1](#).

Flow cytometry

Organoids were removed from BME (R&D Systems), digested with TrypLE (Thermo Fisher) for ~5–10 min into single cells, washed with ice-cold AddMEM/F12 (GIBCO) and filtered into FACS tubes through a cell strainer (Falcon). Prior to FACS, cells were stained with DAPI to identify live cells (Sigma). We performed FACS with analysis buffer that is comprised of 5 mM EDTA, 25 mM HEPES and 1% BSA in DPBS. FACS analysis was performed using the CytoFLEX benchtop flow cytometer (Beckman), and analyzed with FlowJo software. Fluorescent reporter gating strategy in human small intestinal organoids is uniform across this study.

Western blot

Organoids were stimulated with IL-22 for two hours and inhibitors were added to culture medium one hour before IL-22 stimulation. Organoids were collected from BME and washed three times with ice cold PBS. Total protein extract was isolated using RIPA Buffer (50 mM Tris-HCl pH 8.0, 150 mM NaCl, 0.1% SDS, 0.5% Na-Deoxycholate, 1% NP-40, 1X Complete protease inhibitors [Roche]) and protein concentration was measured using a BCA assay kit (Thermo Fisher). Samples were loaded on a pre-cast gradient SDS-PAGE gel 12% (Biorad) and subsequently transferred onto a PVDF membrane (Millipore). The membrane was blocked with 5% milk/BSA in PBST for 1 h prior to incubation with primary antibody. Antibodies used in this study are Phospho STAT3 (Tyr705) (D3A7) XP rabbit antibody, STAT3 (79D7) rabbit antibody, phospho-AKT (ser473) rabbit antibody, Akt (pan) (11E7) rabbit antibody, Phospho-S6 Ribosomal Protein rabbit antibody (Ser235/236), S6 Ribosomal Protein (5G10) rabbit antibody, β -Actin (13E5) rabbit antibody (HRP-conjugated) (Cell Signaling Technology). Secondary antibody used is swine anti-rabbit-HRP (Dako). Membranes were imaged using the Amersham ImageQuant 800 Western blot imaging system.

Transmission electron microscopy

Organoids were chemically fixed for 3 h at room temperature with 1.5% glutaraldehyde in 0.067 M cacodylate buffered to pH 7.4 and 1% sucrose. Samples were washed once with 0.1 M cacodylate (pH 7.4), 1% sucrose and 3x with 0.1 M cacodylate (pH 7.4), followed by incubation in 1% osmium tetroxide and 1.5% K₄Fe(CN)₆ in 0.1 M sodium cacodylate (pH 7.4) for 1 h at 4 C. After rinsing with MQ, organoids were dehydrated at RT in a graded ethanol series (70, 90, up to 100%) and embedded in Epon polymerized for 48 h at 60 C. Ultrathin sections of 60 nm were cut using a diamond knife (Diatome) on a Leica UC7 ultramicrotome, and transferred onto 50 Mesh copper grids covered with a Formvar and carbon film. Sections were post-stained with uranyl acetate and lead citrate. All TEM data were collected autonomously as virtual nanoscopy slide on Tecnai T12 microscopes (Thermo Fisher Scientific, The Netherlands) at 120 kV using an Eagle camera. Data were stitched, uploaded, shared and annotated using Omero and PathViewer. The final pictures were directly acquired at the microscope in a manual standard way using the Eagle camera at 4 kx4k.

Immunohistochemistry staining

Organoids were fixed with 4% paraformaldehyde (PFA) for 1 h at room temperature, washed and dehydrated using an increasing ethanol gradient, and washed in xylene before embedding in paraffin. Paraffin sections were processed with standard techniques. Antibody used in staining on paraffin sections were CHGA (Santa Cruz) and LYZ (Dako), according to manufacturer's instructions. Slides were imaged using a Leica DM4000 microscope.

Confocal imaging

Live organoids with fluorescent reporters were imaged on a Leica Sp8 confocal. Fluorescent images were processed for max projection of all z-stacks using ImageJ software.

Time-lapse imaging

Mechanically dissociated organoids (MUC2-mNeonGreen, DEFA5-IRES-dsRed, CHGA-IRES-iRFP670) were seeded in basement membrane extract (BME, Trevigen) within imaging chambers (day 1). Growth media supplemented with Interleukin was added and refreshed every two days. Time-lapse imaging ran from day 4 to day 7, for ~90 h. The imaging was performed with a scanning confocal microscope (Leica TCS SP8) with a 40x water immersion objective (NA = 1.10). Experiments were performed at 37°C and 5% CO₂. ~30 z-slices with 2 μm step size were taken per organoid every 20 min. At each time point, imaging was conducted in three fluorescence channels, with excitation lasers of 488 nm, 552 nm and 638 nm respectively.

Single-cell tracking and the quantification of fluorescence signal

Cells were manually tracked in 3D using a custom-written imaging analysis software (Kok et al., 2020). Each cell was assigned a unique label at the start of the track. Afterward, the estimated center of mass of the fluorescence signal was followed for each cell. If a cell divided, we noted the labels of both the mother and the two daughter cells, allowing us to obtain lineage trees. We tracked all Paneth cells (DEFA5+), Enteroendocrine cells (CHGA+) and selection of the Goblet cells (MUC2+ only) in each organoid. In order to quantify the fluorescence intensity of single cells, we considered a sphere (diameter = 5 μm) around the tracked location for each cell and at each time point. For all three fluorescence channels, the fluorescence intensity was then calculated as the sum of the fluorescence signal within the sphere divided by the number of pixels in the sphere.

Single-cell transcriptome sample preparation

Organoids were removed from BME (R&D Systems), digested with TrypLE (Thermo Fisher) for 10–15 min into single cells, washed with ice-cold AdMEM/F12 (GIBCO) and filtered into FACS tubes through cell strainer (Falcon) with Rho kinase inhibitor Y-27632 dihydrochloride (10 μM, Abmole Bioscience). Cells were co-stained with DAPI (Sigma) and DRAQ5 (Biostatus) and subjected for FACS sorting of live cells. FACS was performed on BD Influx™ cell sorter (BD Bioscience). 4,000 live cells per condition were subjected to droplet-based scRNA-seq using the 10x Genomics platform. Libraries were prepared using the 10x Genomics Chromium 3' Gene Expression solution v3.1 and sequenced on a NovaSeq6000 (Illumina).

Proteome sample preparation

Organoid material was lysed in 8 M urea, 50 mM ammonium bicarbonate, supplemented with EDTA-free protease inhibitor (cOmplete Mini, Roche Diagnostics). Lysates were cleared by centrifugation at 20,000 g for 1 h at 20°C. Protein content of the supernatant was determined using the Bradford protein assay (Bio-Rad, USA). 30 μg total protein of each sample was diluted with 50 mM ammonium bicarbonate to final volume 100 μL, reduced in 5 mM dithiothreitol (DTT) at 20°C for 1 h and then alkylated in 10 mM iodoacetamide at 20°C for 30 min in the dark. Proteins were then digested at 37°C with Lys-C (Wako, Japan; 1:50 enzyme/protein ratio) for 4 h, followed by trypsin digestion (Sigma; 1:50) overnight at 37°C. 10 μg digested peptides were pre-fractionated off-line, by home-made reversed-phase C18 STAGE tips, using 200 mM ammonium formate, at pH 10. Peptides were separated into 5 fractions using stepped gradients of 11 to 80% acetonitrile, and dried by vacuum centrifugation.

LC-MS/MS analyses

Fractionated peptides were reconstituted in 2% formic acid and triplicate injections of 25% each were analyzed on an Orbitrap Exploris 480 mass spectrometer (Thermo Scientific), coupled to an UltiMate 3000 UHPLC system (Thermo Scientific). Solvents used were 0.1% formic acid in water (Solvent A) and 0.1% formic acid in 80% acetonitrile, 20% water (Solvent B). Peptides were first trapped on a μ-precolumn (C18 PepMap100, 5 μm, 100 Å, 5 mm × 300 μm; Thermo Scientific) in 9% Solvent B, and then separated on an analytical column (120 EC-C18, 2.7 μm, 50 cm × 75 μm; Agilent Poroshell) using a 95-min linear gradient of solvent B per fraction. The resolving gradients for fractions 1 to 5 were 11–20%, 12–28%, 15–34%, 18–35% and 23–40% Solvent B respectively. Eluting peptides were online-injected into the mass spectrometer for data-dependent acquisition. The spray voltage was set to 2.1 kV, the temperature of the ion transfer tube was set to 275°C and a RF lens voltage of 40%. MS scans were acquired at a resolution of 60,000 within the m/z range of 375–1600, accumulating to 'Standard' pre-set automated gain control (AGC) target. Multiply charged precursor ions starting from m/z 120 were selected for further fragmentation. Higher energy collisional dissociation (HCD) was performed with 28% normalized collision energy (NCE), at a resolution of 30,000, and with dynamic exclusion of 16 s and 1.4 m/z isolation window.

QUANTIFICATION AND STATISTICAL ANALYSIS

Single-cell RNA-sequencing data processing

Mapping of sequencing reads

The sequencing output was demultiplexed and converted to FASTQ files using the function *mkfastq* from the CellRanger toolkit (v5.0.1). Reads were then mapped to a custom variant of the GRCh38 human transcriptome in which the endogenous DEFA5 and

MUC2 genes were replaced by the knocked-in tagging constructs (DEFA5-IRES-dsRed and MUC2-mNeonGreen), and feature count tables were generated using the CellRanger *count* function.

Data pre-processing

The output files from CellRanger were read into R (v4.1.0) using the *Read10X* function from the Seurat package (v4.0.3). The percentage of mitochondrial transcripts per cell was calculated and these genes were removed from the expression matrices. A set of cells which were found in a previous analysis to overexpress stress-response genes (“stressed_cells.txt”) were also removed. The expression matrices were then merged, and genes expressed in fewer than 3 cells were filtered. The pre-processed expression matrix was then used to create a Seurat object, and cells with <3,000 unique transcripts, >60,000 unique transcripts or >25% mitochondrial transcript percentage were excluded.

Data integration

To enable the joint analysis of organoid cells cultured under different conditions, we performed data integration as described in (Stuart et al., 2019). Briefly, the full dataset was split by culture condition (+IL-22 and – IL-22) and each resulting object was normalized using the SCTransform method (Hafemeister and Satija, 2019). The genes on which to perform integration ($n = 3000$) were then selected by first taking those deemed variables in both conditions, followed by those with the highest median variable feature rank (wrapped in the *SelectIntegrationFeatures* function). This list was further refined to a set of high-confidence anchor genes used to perform the final data integration (wrapped in *FindIntegrationAnchors* and *IntegrateData*) using the default parameters.

Clustering and differential expression analysis

The top 25 principal components were used to project the integrated data in 2D space via uniform manifold approximation and projection (UMAP) and to perform graph-based cell clustering (Leiden algorithm, resolution of 0.8). Clusters were assigned to known cell types by manual examination of differentially expressed genes (Table S2, Wilcoxon Rank Sum test). To distinguish Paneth cells, we calculated a module score (Tirosh et al., 2016) using the Paneth-specific markers DEFA5, DEFA6, PLA2G2A, PRSS2, REG3A and ITLN2. Cells scoring >1.5 for this gene module were defined as Paneth cells. Tuft cells were distinguished by sub-clustering of the secretory progenitor cluster (*FindSubCluster* function, Leiden algorithm, resolution = 1) and manual examination of Tuft cell marker expression (e.g. AVIL). The cell cycle phase of each cell was inferred using the *CellCycleScoring* function in Seurat. The IL-22-induced module score was calculated using the top 50 upregulated genes (average \log_2 fold-change) in cells cultured in + IL-22 vs – IL-22 medium (Table S3).

RNA velocity analysis

RNA velocity analysis on cells cultured in + IL-22 medium was done using the scVelo python package (v0.2.2, python v3.7) (Bergen et al., 2020). Briefly, input data was filtered to include only genes with 20 shared (spliced and unspliced) counts and log normalized. First and second order moments were calculated per cell using the top 25 integrated principal components and 30 nearest neighbors. RNA velocity was then estimated using the generalized dynamical model and vectors were projected onto the integrated UMAP.

Trajectory modelings

Modeling of differentiation trajectories was done by first projecting cells of interest in DiffusionMaps space, using the top 25 integrated principal components (destiny R package v3.1.1) (Angerer et al., 2016). The top 2 diffusion components were then used as input for trajectory modeling and cell lineage inference using Slingshot (v2.0.0) (Street et al., 2018), specifying the ISC cluster as the starting point for each trajectory. The principal curves calculated for each trajectory were then projected, along with the cells of interest, in DiffusionMaps space to allow for visualization of inferred lineage structure.

Proteome raw data processing

MS data was acquired with Thermo Scientific Xcalibur version 4.4.16.14, and raw files were processed using MaxQuant software version 1.6.15.0 with the integrated Andromeda search engine. Data were searched against the human UniProt database (downloaded in March 2020, containing 188,357 entries) including common contaminants. For all files standard parameter settings were used with enabled the label-free quantification (LFQ) algorithm. Cysteine carbamidomethylation was included as a fixed modification. Protein N-terminal acetylation and methionine oxidation were allowed as variable modifications. Trypsin/P was set as the digestion enzyme (cleaves after lysine and arginine also if a proline follows), and up to two missed cleavages were tolerated. The match-between-run feature was enabled for identification. A false discovery rate (FDR) of 1% was used for peptide and protein identification.

Proteome data analysis

Data were analyzed using Perseus software version 1.6.10.0. LFQ intensities of proteins were \log_2 transformed. Proteins quantified in two out of three replicates in one of experimental conditions were retained for further analysis, after imputation based on normal distribution. To filter for significant changes between experimental conditions, ANOVA test and two-sided unpaired Student's *t* test were performed. FDR-corrected *p* values (*q*-values) were calculated from 250 randomizations and considered significant if they were 0.05 or less (Table S4).

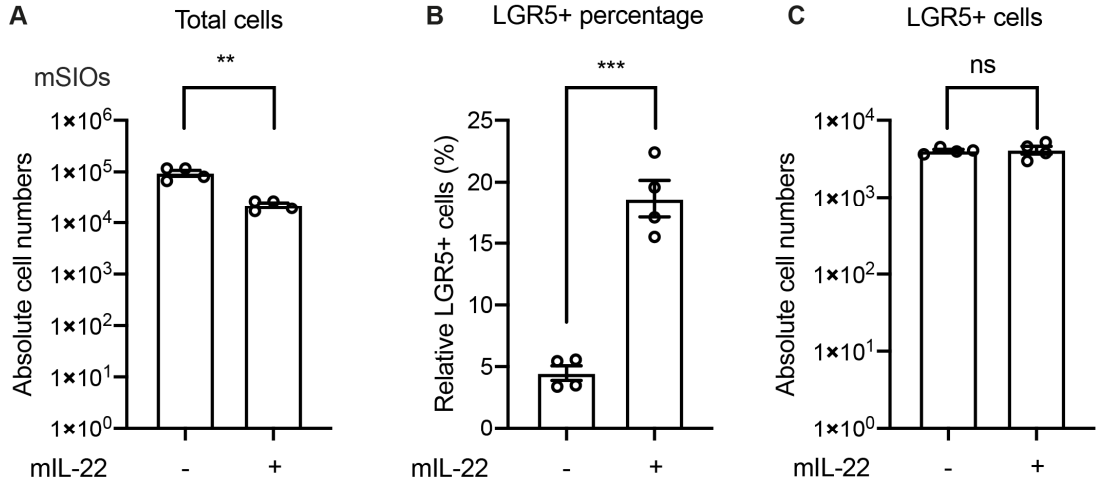
Statistical analysis

Data are presented as means with standard error of the mean (SEM) to indicate the variation within each experiment. Statistics analysis was performed in Prism and R. Two-tailed *t*-test was used for the comparison between two different conditions. For experiments with more than two conditions, ANOVA test was used to calculate significance. Annotation for *p* values in figure legends regardless of statistical test type are: **p* < 0.05, ***p* < 0.01, ****p* < 0.001, *****p* < 0.0001.

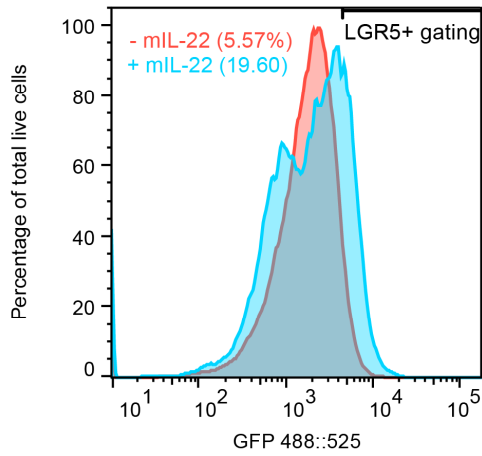
Supplemental Information

Optimized human intestinal organoid model reveals interleukin-22-dependency of paneth cell formation

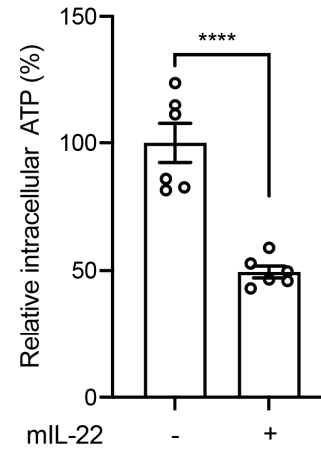
Gui-Wei He, Lin Lin, Jeff DeMartino, Xuan Zheng, Nadzeya Staliarova, Talya Dayton, Harry Begthel, Willine J. van de Wetering, Eduard Bodewes, Jeroen van Zon, Sander Tans, Carmen Lopez-Iglesias, Peter J. Peters, Wei Wu, Daniel Kotlarz, Christoph Klein, Thanasis Margaritis, Frank Holstege, and Hans Clevers



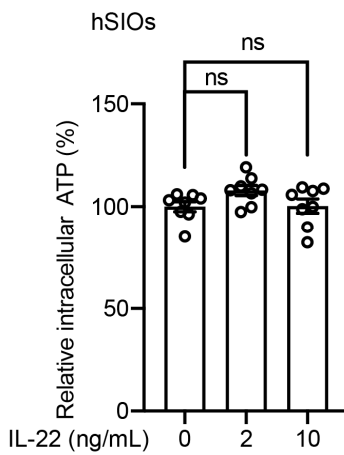
D Representative FACS gating for mouse LGR5+ cell



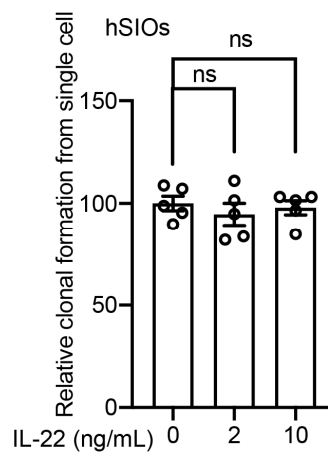
E mSIOs



F Conventional Expansion



G Conventional Expansion



H Conventional expansion

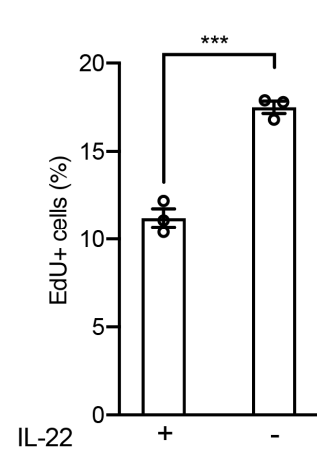


Figure S1. IL-22 does not promote growth of mouse intestinal organoids and conventional cultured human intestinal organoids

(A) Quantification of absolute cell numbers in mouse intestinal organoids cultured in ENR medium with or without the addition mL-22 (5ng/ml) for 7 days. Data are shown as mean \pm SEM. $**P < 0.01$, two-tailed unpaired *t*-test, $n=4$. (B) FACS analysis of relative LGR5+ stem cells in mouse intestinal organoids cultured in ENR medium with or without the addition mL-22 (5ng/ml) for 7 days. Data are shown as mean \pm SEM. $***P < 0.001$; two-tailed unpaired *t*-test, $n=4$. (C) Bar plot showing the absolute number of LGR5+ cells in mouse intestinal organoids cultured in ENR medium with or without the addition of mL-22 (5ng/ml) for 7 days. Data are shown as mean \pm SEM. ns, not significant; two-tailed unpaired *t*-test, $n=4$. (D) FACS gating strategy for mouse LGR5+ cells. (E) Bar plot showing the relative intracellular ATP of mouse intestinal organoids cultured in ENR medium with or without the addition of mL-22 (5ng/ml) for 7 days. Data are shown as mean \pm SEM. $****P < 0.0001$; two-tailed unpaired *t*-test, $n=6$. (F) Bar plot showing the relative intracellular ATP of human intestinal organoids cultured in conventional expansion medium with or without the addition of IL-22 for 7 days. Data are shown as mean \pm SEM. ns, not significant; one-way ANOVA compared with no addition control, $n=8$. (G) Bar plot showing the relative clonal formation efficiency of human intestinal organoids cultured in conventional expansion medium with or without the addition of IL-22 for 7 days. Data are shown as mean \pm SEM. ns, not significant; one-way ANOVA compared with no addition control, $n=5$. (H) Cell proliferation as determined by FACS analysis of EdU positive cells of human intestinal organoids cultured in conventional expansion medium with or without the addition of IL-22 (10ng/mL) for 7 days. Data are shown as mean \pm SEM. *t*-tests using two-stage linear step-up procedure of Benjamini, Krieger and Yekutieli, with $Q=5\%$, $n=3$.

Related to Figure 3.

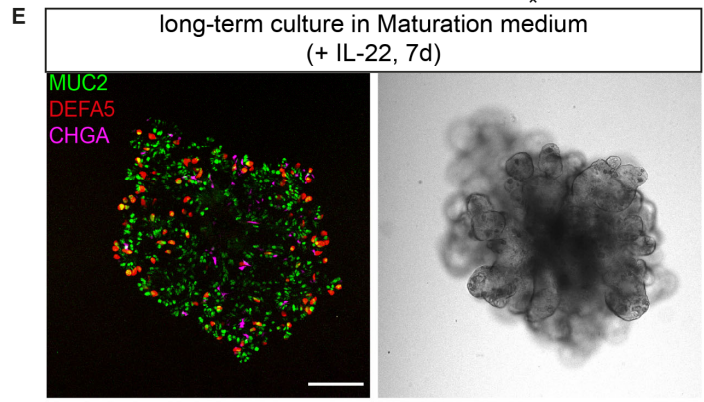
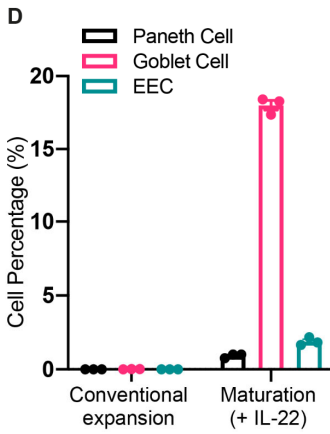
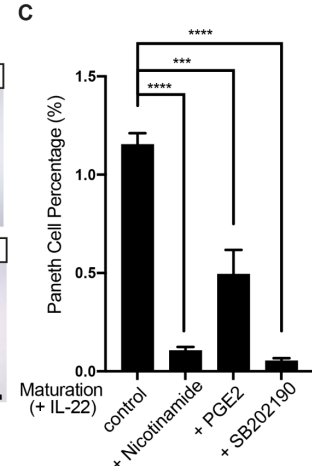
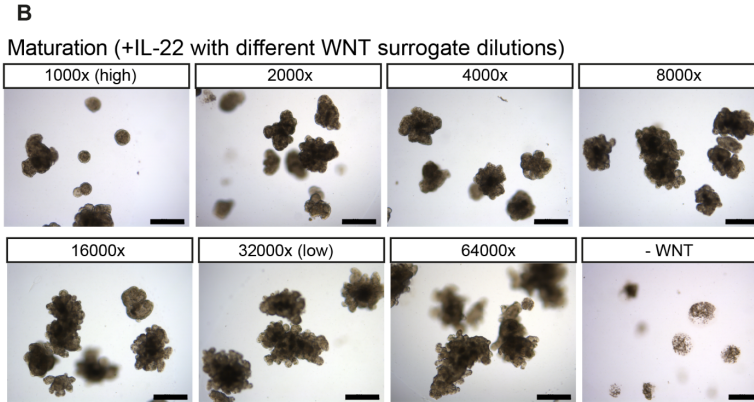
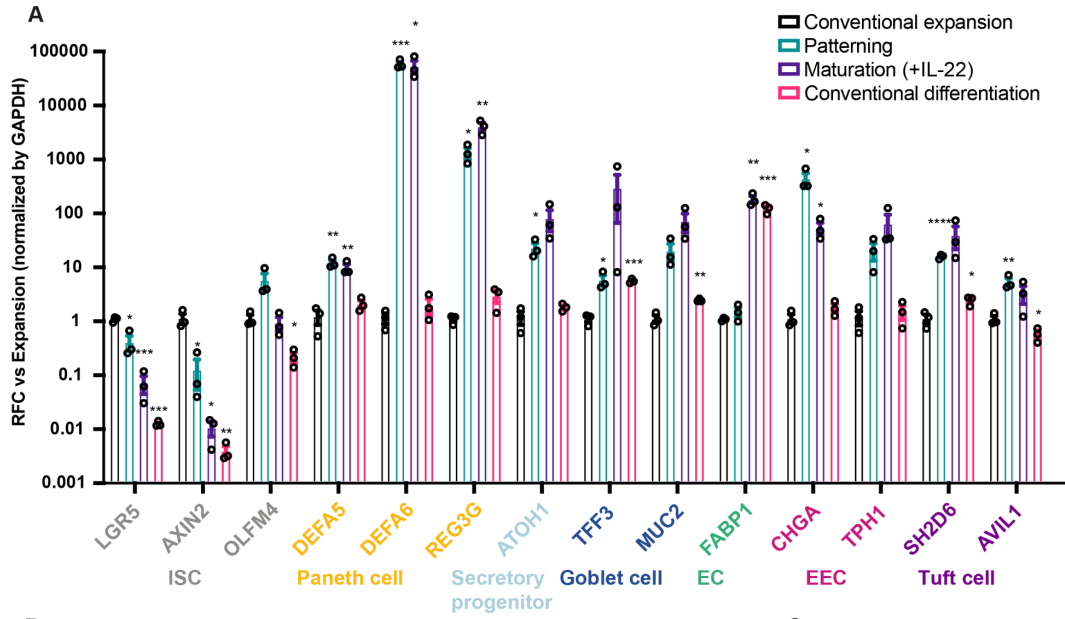


Figure S2. Establishment of an optimal culture model

(A) RT-qPCR quantification of various cell markers in hSIOs cultured in patterning (14 days), maturation medium (+ IL-22) (14 days), conventional differentiation (5 days), and conventional expansion cultures. Data are shown as mean \pm SEM. * P <0.05, ** P <0.01, *** P <0.001, **** P <0.0001; multiple t -tests using two-stage linear step-up procedure of Benjamini, Krieger and Yekutieli, with $Q=5\%$, $n=3$. (B) Representative images of organoids in maturation medium culture (+ IL-22) with different WNT surrogate dilutions in the medium for 14 days. Scale bars, 500 μm . (C) Proportions of Paneth cells as determined by FACS analysis in organoids grown in maturation medium culture (+ IL-22) in the presence of components of the classical culture medium. Data are shown as mean \pm SEM. *** P <0.001, **** P <0.0001; one-way ANOVA compared with maturation medium (+ IL-22), $n=3$ for each condition. (D) Proportions of secretory lineages (Paneth cell, goblet cell and EEC) as determined by FACS analysis in organoids grown in conventional expansion culture and maturation medium culture (+ IL-22) media for 7 days. (E) Representative confocal image of organoids maintained in maturation medium (- IL-22) more than 12 months. IL-22 was added to culture medium 7 days before imaging. Scale bars, 200 μm .

Related to Figure 1.

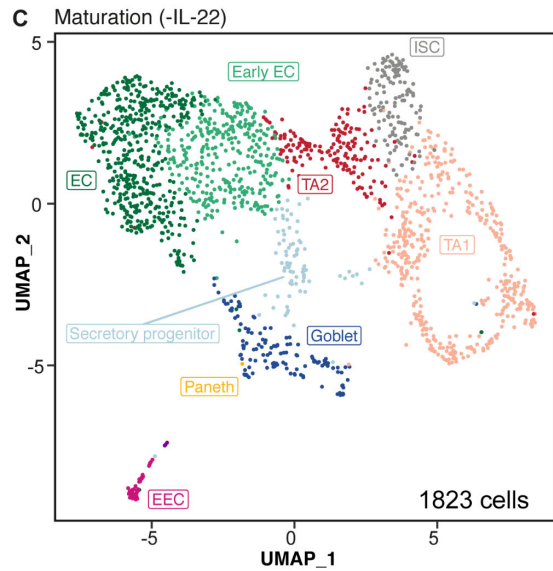
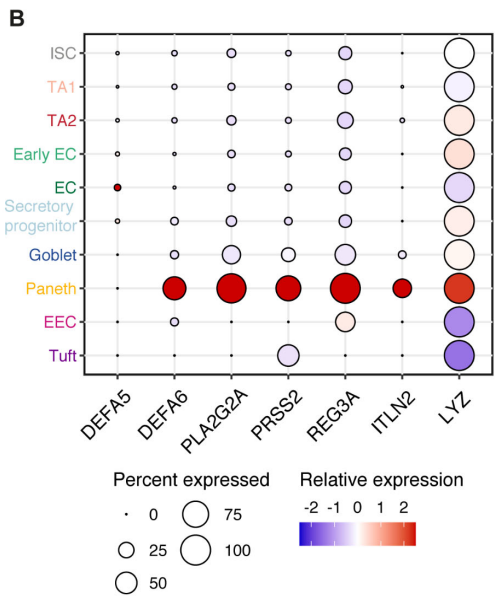
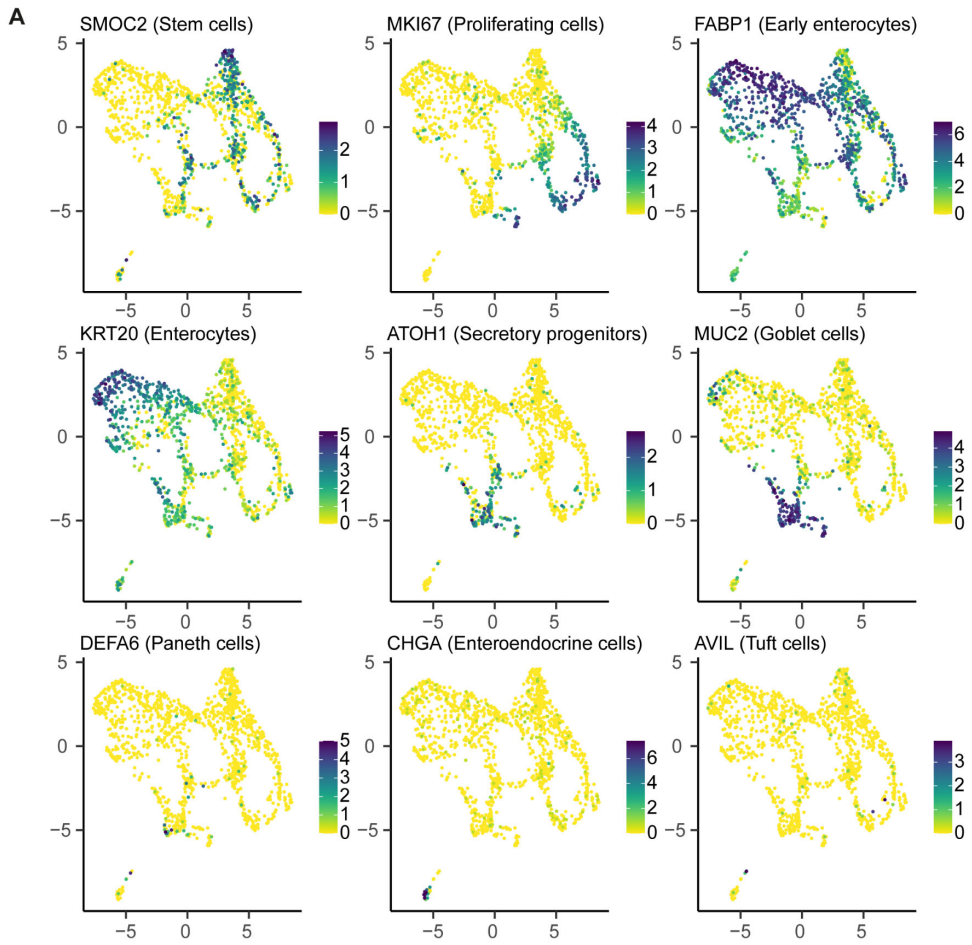


Figure S3. Gene expression by scRNA-seq analysis

(A) UMAP plots showing various cell marker expression levels in maturation medium (+IL-22)-cultured organoids by scRNA-seq. Cells are colored by normalized expression of the indicated genes. (B) Dot plot showing the relative expression and the percentage of cells expressing selected markers across scRNA-seq clusters. (C) UMAP plots showing the integrated scRNA-seq datasets from maturation medium-cultured organoids without IL-22 ($n=1823$ cells).

Related to Figure 2.

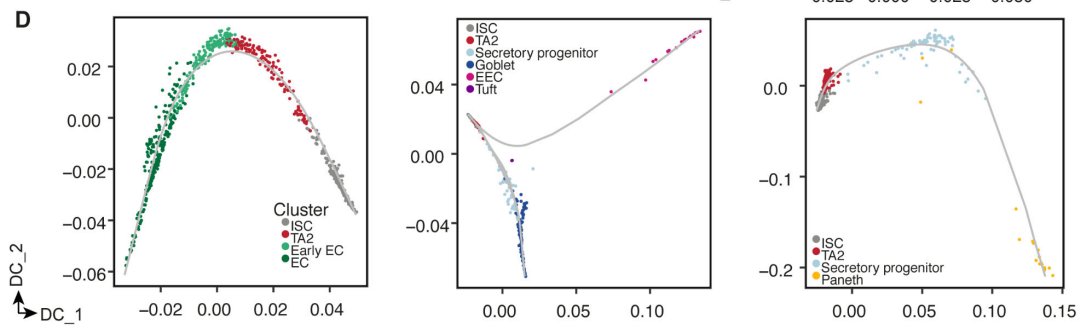
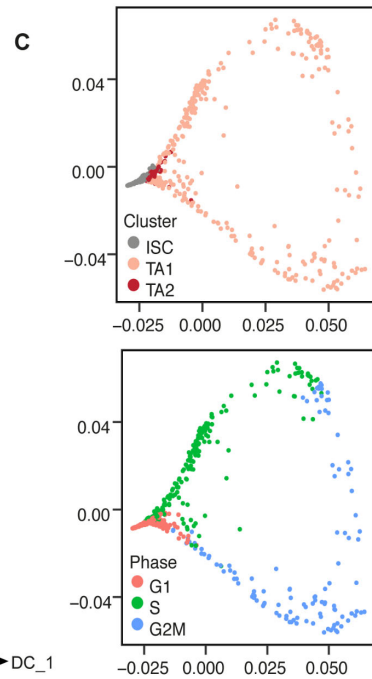
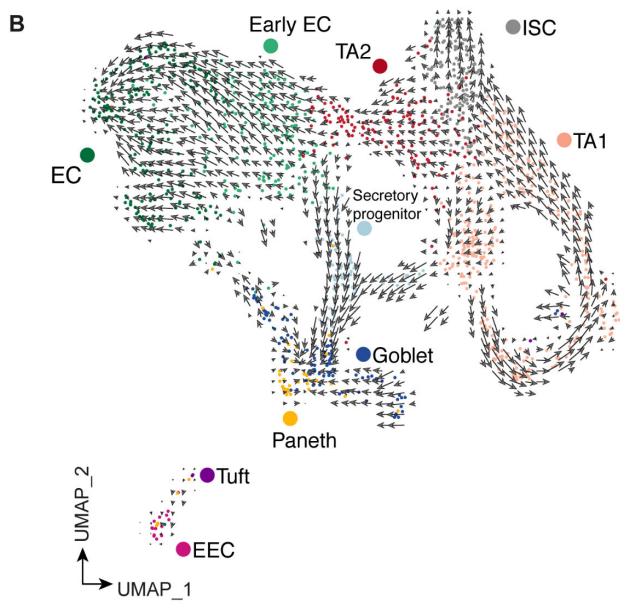
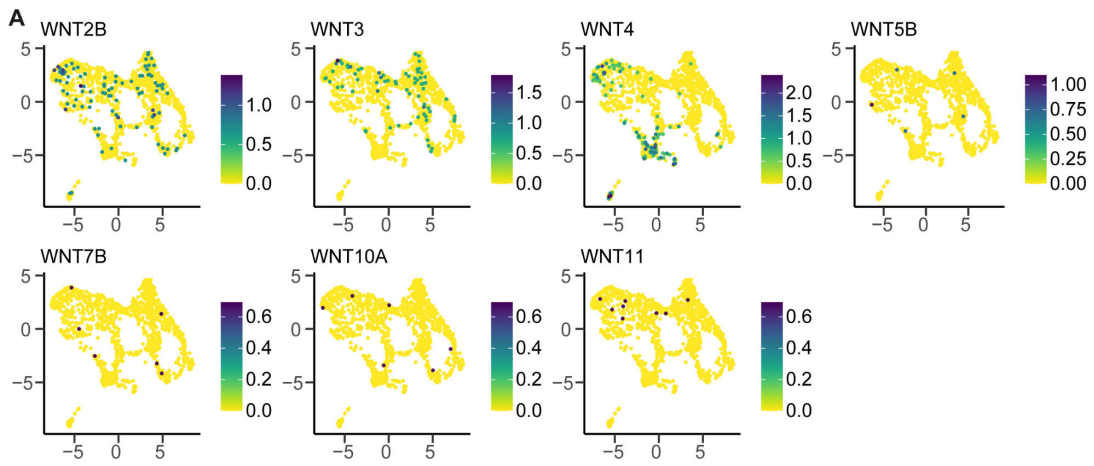
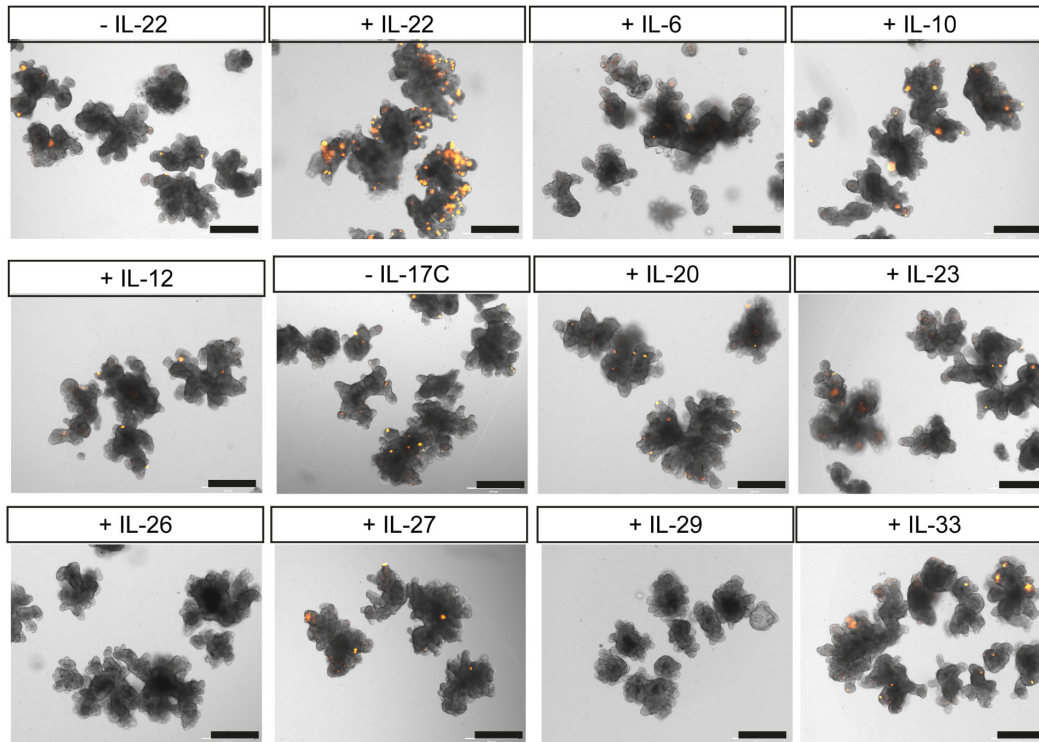


Figure S4. RNA velocity and cell trajectory analysis of scRNA-seq

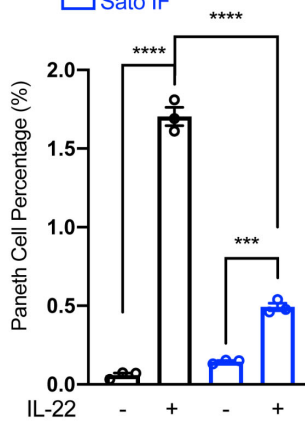
(A) UMAP plots showing WNT gene family expression levels in maturation medium (+IL-22)-cultured organoids that are detected by scRNA-seq. Cells are colored by normalized expression of the indicated genes. (B) RNA velocity vector field calculated by scVelo. Points show cells in UMAP colored according to the respective clusters. Arrows indicate the directionality and magnitude of RNA velocity. (C) Trajectory analysis of the ISCs and TA cells. Each dot plotted in DiffusionMaps space was colored according to its cell type (left) and cell division phase (right). (D) Trajectory analysis of the absorptive lineage (left), secretory lineage excluding Paneth cells (middle) and Paneth cells (right). Each dot plotted in DiffusionMaps space was colored according to its cell type.

Related to Figure 2.

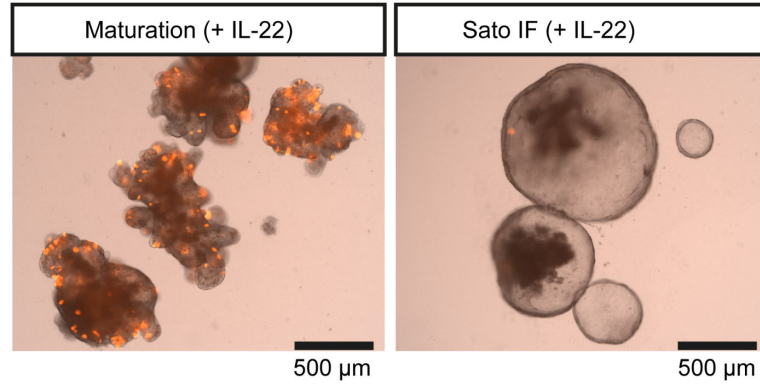
A Maturation



B Maturation medium
 Sato IF



C



D IL10RB IBD variants

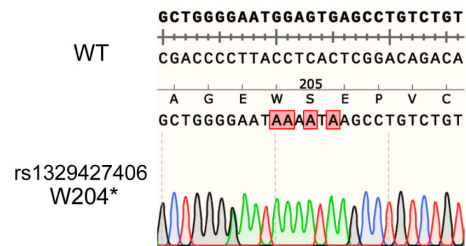
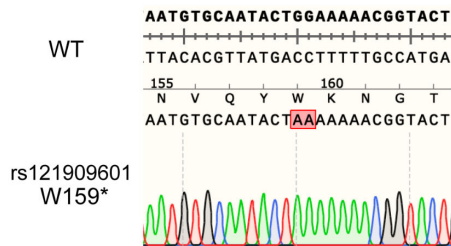


Figure S5. IL-22 induces Paneth cell differentiation in hISOs

(A) Representative images of maturation medium-cultured organoids in response to different cytokines for 7 days. IL-22 (2ng/mL); IL-6 (10ng/mL); IL-10 (10ng/mL); IL-12 (10ng/mL); IL-17C (10ng/mL); IL-20 (10ng/mL); IL-23 (10ng/mL); IL-26 (10ng/mL); IL-27 (10ng/mL); IL-29 (10ng/mL); IL-33 (10ng/mL). Scale bars, 500 μ m. (B and C) Organoid maintained in our maturation media (-IL-22) were replated and cultured with indicated conditions for two weeks. (B) Proportions of Paneth cells determined by FACS analysis. Data are shown as mean \pm SEM. *** $P < 0.001$, **** $P < 0.0001$; multiple t -tests using two-stage linear step-up procedure of Benjamini, Krieger and Yekutieli compared with $Q = 5\%$, $n = 3$ for each condition. $n = 3$ for each condition. (C) Representative images of organoids cultured with Maturation (+IL-22) medium and Sato IF medium (+IL22). (D) Representative genotypes of clonal hSIO lines with CD-associated IL10RB deficient variants.

Related to Figure 4 and 5.

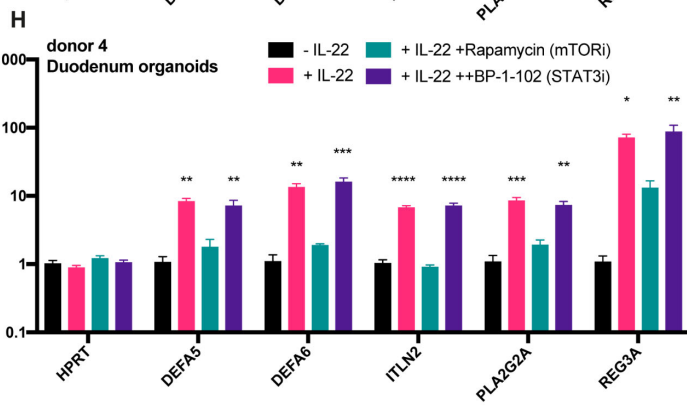
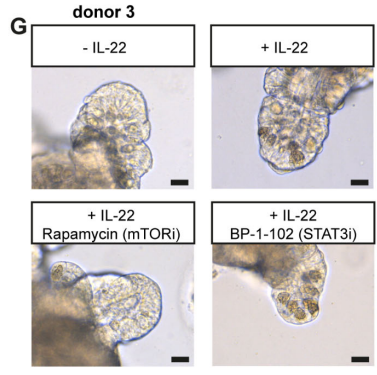
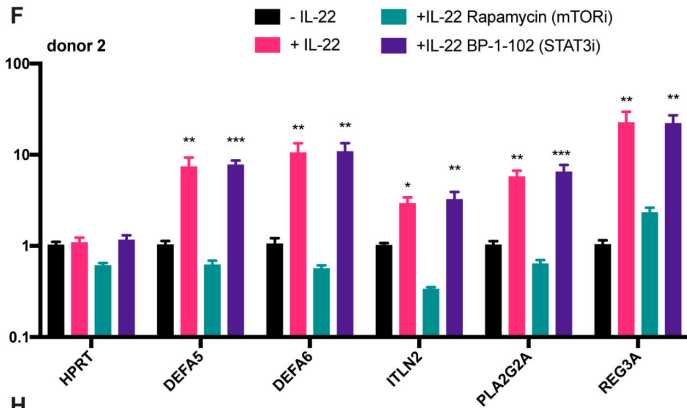
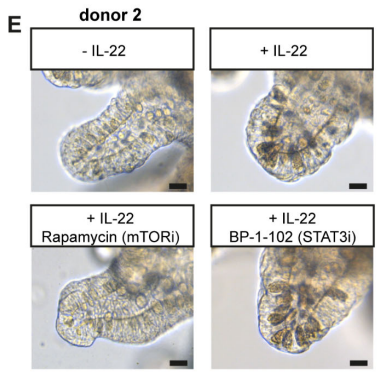
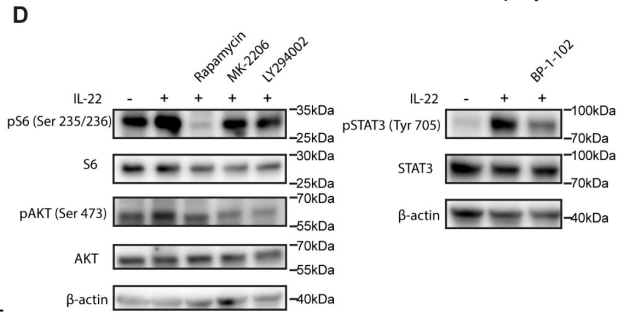
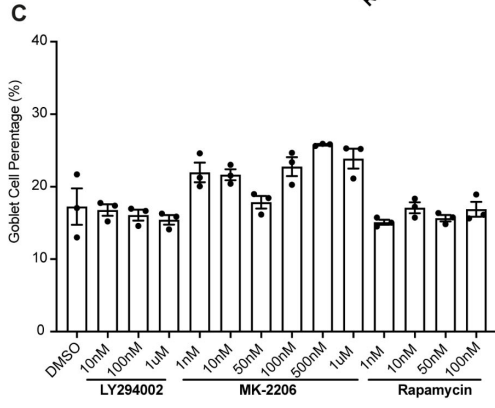
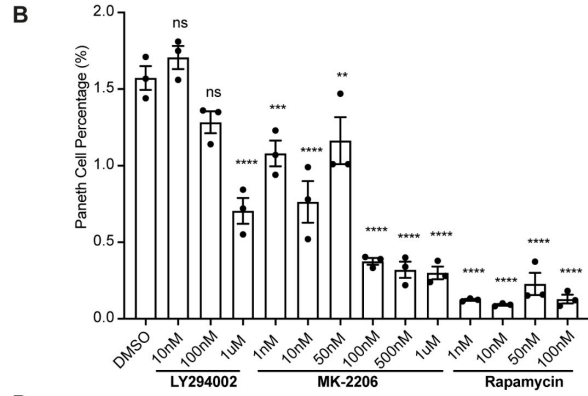
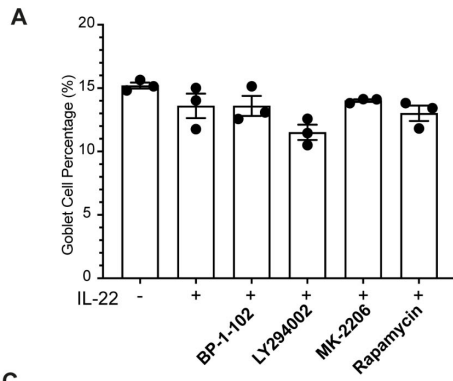


Figure S6. IL-22 induces Paneth cell differentiation through PI3K/Akt/mTOR axis

(A) Proportions of goblet cells as determined by FACS analysis in maturation medium-cultured organoids by MUC2-mNeon reporter with different treatments for 7 days. (B and C) Proportions of Paneth cells (DEFA5- IRES-DsRed reporter) (B) and goblet cells (MUC2-mNeon reporter) (C) as determined by FACS analysis in maturation medium-cultured organoids with different dosages of small molecule inhibitors for 7 days. Data are shown as mean \pm SEM. ns, not significant, $**P<0.01$, $***P<0.001$, $****P<0.0001$; one-way ANOVA compared with DMSO control, $n=3$ for each treatment. (D) Immunoblots of organoids showing the activation of mTOR and STAT3 signaling in response to IL-22 treatments and inhibitor treatments. Organoids were stimulated with IL-22 and given inhibitor for 2 hours. (E and G) Representative zoom-in images of budding crypts of maturation medium-cultured organoids from additional two donors in response to different treatments for 7 days. Scale bars, 20 μm . (F and H) RT-qPCR quantification of human Paneth cell-associated gene expression in response to different treatments in organoids from additional two donor for 7 days. Data are shown as mean \pm SEM. $*P<0.05$, $**P<0.01$, $***P<0.001$; one-way ANOVA compared with maturation medium-cultured organoids (- IL-22), $n=3$ for each treatment.

Related to Figure 6.

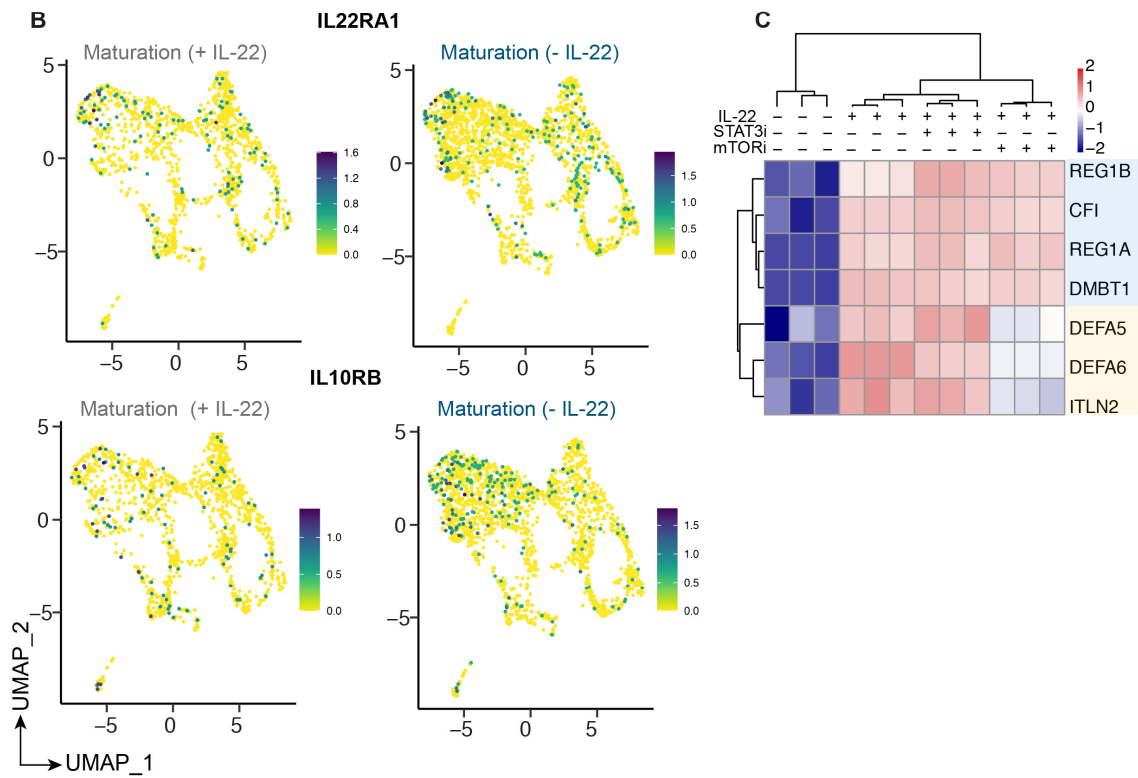
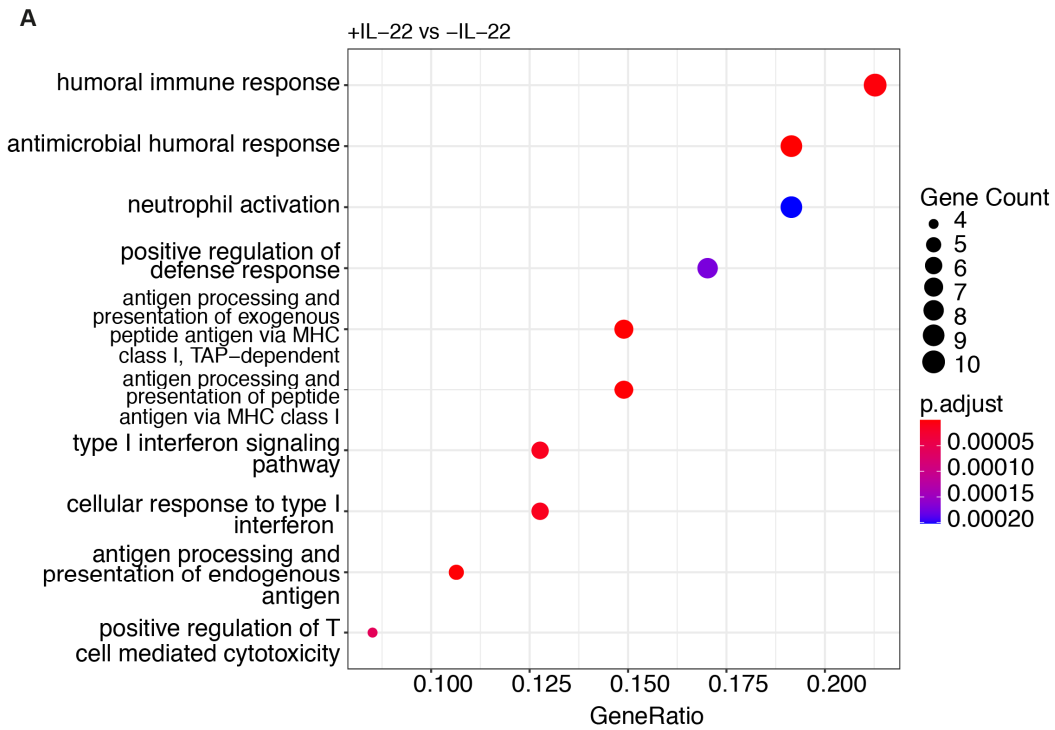


Figure S7. IL-22 induces unique gene expression signature

(A) Selected GO terms (top 10) of differential gene expressions in maturation medium-cultured organoids with versus without IL-22 (pseudo bulk, top 50 genes ranked by Average \log_2FC , Wilcoxon rank sum test). (B) UMAP plots showing the expression of IL-22 receptors, IL22RA1 and IL10RB, in maturation medium-cultured organoids with or without IL-22 by scRNA-seq. Cells are colored by normalized expression of the indicated genes. (C) Heat map representation of the proteins upregulated by IL-22 treatment for 3 days but reversed or not reserved by rapamycin. Scale represents scaled protein abundance and ranges from low (blue) to high (red).

Related to Figure 7 and Table S4.